MAX-PLANCK-INSTITUT FÜR PLASMAPHYSIK

GARCHING BEI MÜNCHEN

Magnetohydrodynamic Instabilities for Tokamaks With Noncircular Cross Section

W. Kerner*

IPP 6/134 March 1975

* Present address: Princeton University, Plasma Physics Laboratory, Princeton, N.J. 08540, USA

Die nachstehende Arbeit wurde im Rahmen des Vertrages zwischen dem Max-Planck-Institut für Plasmaphysik und der Europäischen Atomgemeinschaft über die Zusammenarbeit auf dem Gebiete der Plasmaphysik durchgeführt.

ABSTRACT

The stability behavior of a class of exact tokamak equilibria is investigated in the context of ideal magnetohydrodynamics. The equilibria have an almost constant volume current in the toroidal direction and also a poloidal current which produces a diamagnetic or paramagnetic current distribution. The plasma cross sections are roughly elliptic. The plasma is surrounded by a vacuum extending to a perfectly conducting wall.

Stability is investigated by means of the energy principle. Suitable test functions are used to detect unstable perturbations and to determine the respective growth rates. The calculation involves no approximations, and so all parameters of the equilibrium solution can be arbitrarily varied. In this method only the stability limit is undetermined. With a free plasma boundary instabilities occur below and above the Kruskal-Shafranov limit for every aspect ratio investigated (i.e., $\epsilon^{-1} > 5$). Equilibria with highly elliptic cross sections generally involve more instabilities than those with circular cross sections. In order to attain a high degree of accuracy, extensive algebraic calculations are done by computer using the REDUCE programming language.

CONTENTS

INTRODUCTION

This paper treats the stability of a class of exact axisymmetric plasma equilibria of the tokamak type in the context of ideal magnetohydrodynamics. The equilibria discussed have an almost constant volume current in the toroidal direction and a poloidal current which produces a diamagnetic or paramagnetic current distribution. In addition, there is a toroidal magnetic field generated by an external current. The inverse aspect ratio ϵ is variable. The plasma cross sections are roughly elliptic having arbitrary ratio of half axes. The Garching belt pinch with an ratio of half axes of 10 to 1 can be approximately described with these equilibria. A very interesting question is whether shaped cross sections in tokamak discharges afford an advantage in form of an improved stability behavior, a higher value for the plasma beta, β_T, or a higher current density in comparison with the circular cross section used so far. The physical system investigated consists of a plasma surrounded by a vacuum extending to a perfectly conducting wall, the wall-to-plasma distance being varied.

First, the results of previous stability investigations relevant to our problem are discussed. The energy principle [1] to [3] often used here which implies minimization of a functional δW (variation of the potential energy), is equivalent to solving the linearized MHD equations.

In [4] the possibility of stabilizing a circular cylindrical plasma with a uniform axial magnetic field and a perfectly conducting wall is investigated. The axial magnetic field in the plasma and vacuum may be different. In an

equilibrium with surface current complete stability can be achieved if the wall is sufficiently close to the plasma and the magnetic fields are appropriately chosen. This is no longer possible in an equilibrium with constant axial volume current. The best that can be accomplished is a reduction of the instability ranges and of the growth rates of the perturbations.

In [5], cylindrical equilibria with elliptic cross section, uniform axial magnetic field and constant axial volume current are treated. In the limit of low pressure and long-wave perturbations a general solution is found by using the energy principle and introducing elliptic cylindrical coordinates. Increasing ellipticity then produces more instabilities.

For toroidal equilibria with surface currents the energy integral can be converted to a surface integral over the plasma-vacuum interface. It is then possible to compute the minimum of δW and hence the stability limit [7], [8], [9] by computer.

In [7], a plasma with circular cross section that is surrounded by a perfectly conducting wall is investigated. The equilibrium is numerically calculated by an iterative method. The stability ranges are plotted for various values of the plasma, wall and torus radii. The closer the wall is to the plasma the more stable are the configurations.

In [8], the equilibrium is also determined for a circular plasma cross section, by means of an expansion in ϵ. If β_T/ϵ exceeds a critical value, instabilities occur above and below the Kruskal-Shafranov [20] limit. In this case the toroidicity has a destabilizing effect for long-wave perturbations.

A perfectly conducting wall concentric with the plasma then has a stabilizing effect only if it is very close to the plasma.

In [9], only straight systems are dealt with. The method can also be extended to toroidal configurations by means of an expansion in ϵ. Equilibria with various cross sections, including the belt pinch, are investigated, the stability calculation being restricted to long-wave perturbations. The cross section most favorable for stability is the circle.

In [10], the effect of the toroidal curvature on the stability of tokamak configurations is investigated with an expansion in ϵ. This shows that the toroidal curvature intensifies the instabilities. It is only when a perfectly conducting wall is located immediately at the plasma that the torus improves stability.

The energy integral is used in [11] to derive a sufficient criterion for stability to perturbations which do not affect the plasma boundary. The application [12] to axisymmetric equilibria in the vicinity of the magnetic axis (i.e., for small ϵ) shows favorable stability behavior for D-shaped plasma cross sections with a diamagnetic poloidal current.

For the numerical treatment of two-dimensional equilibria it is assumed in [13], [14], and [15] that the plasma boundary remains unperturbed. This yields a simplified problem without a vacuum region. The energy principle is again used in [13] and [14]. An expansion of the perturbations into a complete system of functions in one [14] and two [13] variables is made to formulate an eigenvalue problem which is solved by computer. These two methods have only been successful in the respective simple special case so far.

The stability of cylindrical plasmas is studied in [15]. For this purpose the linearized MHD equations are numerically solved by computer as an initial boundary value problem. The method is applied to an equilibrium with axial volume current and rectangular cross section. An arbitrary initial perturbation is taken as a basis to find the dominating instability which overrides all stable oscillations after a certain time. The instability regions and growth rates of the perturbations become larger as the axis ratio of the rectangle increases.

Good numerical methods are available for calculating axisymmetric equilibria, e.g. [16]. Required then is a method of determining the instabilities for every equilibrium thus calculated. This is the aim of the methods in [13], [14], and [15]. In two-dimensional stability investigations, only possible with large computers, the computing accuracy is decisive for their basic feasibility. Using the energy principle one requires for the functional δW, which assumes mainly positive values, the regions with negative values and, for marginal stability, the zero. Difficulties occur particularly with instabilities having a small growth rate because very small differences between very large numbers are calculated. The more complicated the equilibrium and the more extensive the minimization procedure the larger is the error due to cancellations. Similar difficulties are created by the rounding errors in a numerical calculation of the MHD equations by a difference method, e.g., [15]. The error in a numerical calculation is never smaller than that in the input data. This means that the error in the equilibrium solution which is calculated numerically or by an approximation method may already be too large for the stability calculation.

Toroidal equilibria with volume current have so far only been approximately treated. In order to establish whether the results of the studies discussed are valid for the tokamak, let us state the critical points:

1. Validity of the surface current model.
2. Restriction to perturbations with fixed boundary.
3. Perfect conductivity of the wall.
4. Validity of the expansion in the inverse aspect ratio.

Here it should be noted:

Re 1. A volume current is needed in the tokamak because of the Ohmic heating. The significance of the surface current model rests in the large number of configurations treated, not in the realistic description of the tokamak.

Re 2. The plasma boundary can be maintained with a wall or limiter, these being destroyed, however, on contact with the hot plasma. This produces impurities in the plasma, thus cooling it. From the experimental point of view it is desirable to have configurations which confine the plasma just with magnetic fields, and which therefore have a free boundary. In general, instabilities which change the boundary have the highest growth rates and are therefore the most dangerous in practice.

Re 3. As the wall has only finite conductivity, stabilization is less favorable than in the idealized case (see [17]), particularly for long confinement times. Calculations with a perfectly conducting wall allow to estimate

the growth rates for the finite-conductivity case according to [18]. – At a large distance from the plasma the wall has no influence.

Re 4. Despite the known MHD instabilities it is assumed that the tokamak can be operated in a regime not far from marginal stability, in so-called stability windows. Owing to the accuracy required for a small aspect ratio and small growth rates it is not clear whether expansion is permissible and in what order this expansion has to be truncated. Critically speaking, no sufficiently reliable solution of the stability problem has yet been found for the tokamak.

With a limited objective we will now derive results valid for the tokamak. This means that the stability investigation for the exact equilibria given has to be performed in such a way that none of the restricting assumptions 1, 2, and 4 is used. According to the energy principle the detection of instabilities with so-called test functions which make δW negative [2], [3] is exact. The use of suitably chosen test functions considerably simplifies the stability problem. Only the stability limit is then undetermined. The instabilities found occur in the tokamak experiments. In this way we see which equilibria have particularly poor stability qualities. These results may, furthermore, improve our understanding of the causes of the MHD instabilities involved.

This report represents a continuation of the stability calculation made by Küppers, Pfirsch, and Tasso [6].

These authors treat an exact axisymmetric equilibrium with circular plasma cross section, almost constant volume current and free boundary. The

test functions are taken from the cylinder solution [4]. The extensive algebraic calculations are performed by computer using the programming language REDUCE. It is proved that instabilities exist above and below the Kruskal-Shafranov limit.

The equilibrium treated in [6] is contained in our class of equilibria. To achieve a high degree of accuracy, coordinates adapted to the equilibrium are introduced as in [6], thus allowing analytic integration of δW in two dimensions. The metric tensor can be expressed with simple functions if non-orthogonal coordinates, perpendicular to the toroidal direction, are used. All quantities then have to be written in covariant form. The extensive algebraic calculations are done by computer using the REDUCE program system [28] and [29].

The ansatz for the test functions is chosen by analogy with the eigenfunctions of the corresponding cylindrical equilibria [4] and [19]. The solution [5] is not used since it was not known at the beginning of this study and since the elliptic coordinates used in [5] are not suitable for our calculation.

Compared with [6] the test functions are modified for ellipse-like cross sections and generalized with a Fourier series. A number of free constants are introduced and determined by minimization of δW with respect to these constants. We thus improve the ansatz for the test functions with a minimization.

We give the growth rates of the unstable perturbations, which can be estimated with the energy principle.

The accuracy required of all calculation steps for the concluding numerical calculation is taken into account. In this way we want to find the conditions for an extended minimization of δW and for the solvability of the stability problem in general, also with respect to other equilibria.

Very little experience in handling extensive algebraic calculations by computer is as yet available. A good deal of the work is therefore concerned with the programming of the problem.

The equilibrium and the related quantities are derived in Sec. I. Section II describes the ansatz for the test functions and the performing of the stability calculation. The results obtained are presented in Sec. III.

The description of the computational program is given in Sec. II. 4. For more details on the code see [21] . Reference [21] puts the emphasis on the algebraic manipulation which is fundamental to calculation.

I. EQUILIBRIUM

I.1 Derivation of Equilibrium

For the derivation of axisymmetric, magnetostatic equilibria it is convenient to use cylindrical coordinates r, ϕ, z. Because of axisymmetry all terms are independent of the toroidal direction ϕ. Furthermore, the magnetic field $\vec{B}$ is expressed by the flux function ψ and a quantity T:

I.1 $$T = B_\phi \cdot r \ ,$$

I.2 $$\vec{B} = \nabla\phi \times \nabla\psi + T\nabla\phi \ .$$

For the current density $\vec{j}$ we get from the Maxwell equation $\vec{j} = \nabla \times \vec{B}$ the following expression:

I.3 $$\vec{j} = \{ r^2 \, \mathrm{div}\,(\nabla\psi/r^2)\}\,\nabla\phi + \nabla T \times \nabla\phi \ .$$

It holds that the pressure p and the quantity T depend only on the surface, i.e., $p = p(\psi)$ and $T = T(\psi)$. The static equation of motion is

I.4 $$\frac{\partial^2\psi}{\partial r^2} - \frac{1}{r}\frac{\partial\psi}{\partial r} + \frac{\partial^2\psi}{\partial z^2} = -r^2\frac{dp}{d\psi} - T\frac{dT}{d\psi} \ .$$

Making the choice for p and T

I.5 $$p = p_o - p'\psi \ ,$$

I.6 $$T^2 = T_o^2 + 2\gamma\,\frac{p'}{1+\alpha^2}\,\psi \qquad p_o,\ p',\ \alpha,\ T_o,\ \gamma \text{ are constants with } p' > 0 \ ,$$

we get a particular solution of Eq. I.4 [6]

I.7 $$\psi = [z^2(r^2 - \gamma) + \frac{\alpha^2}{4}(r^2 - R^2)^2]\,\frac{p'}{2(1+\alpha^2)} \ ,$$

where R is the distance from the symmetry axis to the magnetic axis. For the stability analysis with these equilibria a coordinate system which uses

the flux surfaces as one coordinate and the toroidal angle as another coordinate is especially adapted.

While it is very difficult to determine the appropriate orthogonal coordinates, we are able to give non-orthogonal coordinates X^1, X^2, X^3 as in [6] .

I.8
$$X^1 = \left\{ \left[z^2 \cdot (r^2 - \gamma) + \frac{\alpha^2}{4} (r^2 - R^2)^2 \right] \frac{1}{\alpha^2} \right\}^{1/2}$$

$$X^2 = \phi$$

$$X^3 = \text{Arctg} \left(\frac{2}{\alpha} \frac{z (r^2 - \gamma)^{1/2}}{r^2 - R^2} \right) .$$

The innermost surface $X^1 = 0$ describes the magnetic axis. X^3 denotes the angle on the flux surfaces in a plane $X^2 = ct.$ The following outline illustrates the situation:

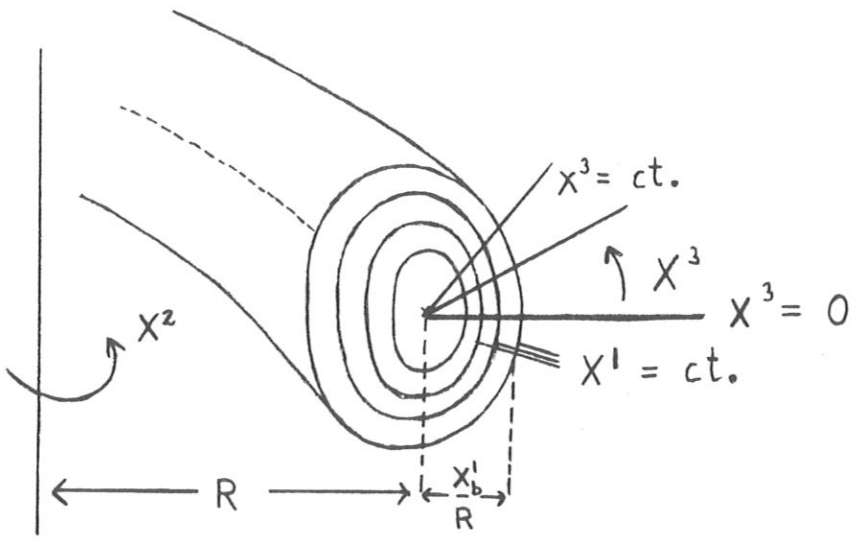

Using $r^2 = x^2 + y^2$, we can express X^1, X^2, X^3 by x, y, z and vice versa.

$$x = r \cos X^2 \qquad r = (2X^1 \cos^3 + R^2)^{1/2}$$

$$y = r \sin X^2$$

$$z = \frac{\alpha X^1 \sin X^3}{(r^2 - \gamma)^{1/2}}$$

For evaluation of all metric quantities and of the covariant and contravariant components of vectors respectively, we need the

$$b_i^k = \frac{\partial x^k}{\partial X^i} \qquad i, k = 1, 2, 3$$

In a known manner [6] and [22], we obtain for the covariant components of the metric tensor:

$$g_{11} = \frac{1}{r^2 - \gamma}\left[\frac{r^2 - \gamma}{r^2}\cos^2 X^3 + \alpha^2 \sin^2 X^3 + \frac{\alpha^2 X^1 \sin^2 X^3}{r^2 - \gamma}\left(\frac{X^1 \cos^2 X^3}{r^2 - \gamma} - 2\cos X^3\right)\right],$$

$$g_{12} = g_{21} = 0 \quad ,$$

$$g_{13} = g_{31} = \frac{X^1}{r^2 - \gamma}\left\{\left(\alpha^2 - \frac{r^2 - \gamma}{r^2}\right)\sin X^3 \cos X^3 + \frac{\alpha^2 X^1 \sin X^3}{r^2 - \gamma}\left[\left(\sin^2 X^3 - \cos^2 X^3\right) - \frac{X^1 \sin^2 X^3 \cos X^3}{r^2 - \gamma}\right]\right\},$$

I.9

$$g_{22} = r^2 \quad ,$$

$$g_{23} = g_{32} = 0 \quad ,$$

$$g_{33} = \frac{(X^1)^2}{r^2 - \gamma}\left[\frac{r^2 - \gamma}{r^2}\sin^2 X^3 + \alpha^2 \cos^2 X^3 + \frac{\alpha^2 X^1 \sin^2 X^3}{r^2 - \gamma}\left(2\cos X^3 + \frac{X^1 \sin^2 X^3}{r^2 - \gamma}\right)\right],$$

$$\sqrt{g} = \sqrt{\det(g_{ij})} = \frac{\alpha X^1}{\sqrt{r^2 - \gamma}} \quad .$$

The contravariant components of the magnetic field and of the current density are:

$$B^1 = 0 \quad ,$$

$$B^2 = \frac{1}{r^2}\, T(X^1) \quad ,$$

$$B^3 = -\frac{\alpha p'}{1+\alpha^2}\sqrt{r^2 - \gamma} \quad , \qquad T_o = R \cdot B_o \, ; \quad B_o = \text{ct.}$$

I.10

$$J^1 = 0 \quad , \qquad T_\psi = \frac{dT}{d\psi} = \frac{\gamma p'}{T(1+\alpha^2)}$$

$$J^2 = p'\left(1 - \frac{\gamma}{r^2(1+\alpha^2)}\right) \quad ,$$

$$J^3 = T_\psi \frac{\alpha p'}{1+\alpha^2}\sqrt{r^2 - \gamma} \quad ,$$

Since the pressure vanishes on the plasma boundary described by $X^1 = X^1_b = \text{constant}$, we get an additional relation between the constants,

$$p' = \sqrt{\frac{2(1+\alpha^2)}{\alpha^2}}\, \sqrt{p}_o \, \frac{1}{X^1_b} \quad .$$

The ratio of small and large plasma radius – the inverse aspect ratio – is

$$\text{I.11} \qquad \epsilon = \frac{\Delta r}{R} = \frac{X^1_b}{R^2} \quad ,$$

if $(X^1_b/R^2) < 1/2$ is assumed. For X^1_b/R^2 near to $1/2$, it has the value

$$\epsilon = \frac{2X^1_b}{R^2} \approx 1 \, .$$

Near the magnetic axis the quantity α is connected with the ratio of half axes of the flux surfaces

I.12 $$e = \frac{\alpha}{\sqrt{1-\delta}} \quad , \qquad \text{if we set} \qquad \gamma = \delta R^2 \; .$$

We call the current distribution in I.10 diamagnetic if the toroidal magnetic field increases with X^1. Then configurations with positive values for $\gamma = \delta \cdot R^2$ are diamagnetic, and those with negative values for γ paramagnetic.

An analytical solution for ψ in the vacuum region fulfilling the boundary conditions for ψ and $\vec{B}$ on the plasma boundary cannot be given. For cylindrical equilibria, however, the solution is known [23]. The singularities of $\vec{B}_{vac}$ determine the position and the value of the currents being necessary to maintain the equilibrium and flowing in additional conductors in the vacuum.

We assume that the plasma is surrounded by vacuum and a perfectly conducting wall. It is possible to use the energy principle even if the wall is not a magnetic surface in the vacuum region. We, therefore, assume that the wall is situated on a surface $X^1 = \text{const} \geq X^1_b$. The exact solution for the vacuum region can give an upper limit for the possible distance of the wall surface $X^1 = \text{const}$ from the plasma boundary. For inside this surface, there cannot be a singularity.

The coordinates X^1, X^2, X^3 can be used only in the region $0 \leq X^1 \leq X^1_{Gr}$, since otherwise there exist poles in the g_{ij} (see I.9). The

boundary surface is determined by the stagnation points of the magnetic field. In cylindrical coordinates these points are given by the formulae

$$\frac{\partial \psi}{\partial r} = 0 \qquad \text{and} \qquad \frac{\partial \psi}{\partial z},$$

with

$$r = R\sqrt{\delta} \qquad \text{and} \qquad z = \pm R \cdot \alpha \sqrt{\frac{1-\delta}{2}} \quad ,$$

if $1 > \delta \geq 0$. The boundary surface is given by $X^1_{Gr} = (1-\delta) \cdot R^2/2$.

The following diagrams 1 to 3 show flux surfaces and stagnation points with different values for the constants α and δ. While the parameter α influences the ratio of half axes of the cross section, the parameter δ varies the surfaces into a D-shaped form.

I.2 Evaluation of q and β

We evaluate the safety factor $q = q(\psi) = (2\pi/i)$

$$q = \left(\frac{d\chi}{2\pi\, d\psi}\right) \quad ,$$

where $2\pi\psi$ is the azimuthal magnetic flux, and χ the longitudinal flux through a flux surface

$$\chi(X^1) = \int_0^{X^1} dX'^1 \int_0^{2\pi} dX^3 \, \frac{\alpha X'^1}{(r^2-\gamma)^{1/2}_r} \, \frac{T}{r} \quad .$$

Expanding the denominator into a Taylor series we can perform the integration with respect to X^3 analytically

$$R_\gamma = R\sqrt{1-\delta}$$

$$\chi(X^1) = \frac{2\pi\alpha}{R^2 R_\gamma} \int_o^{X^1} dX'^1 X'^1 T(X'^1) \left[1 + \sum_{v=2,4,6\ldots} t_\nu \left(\frac{X'^1}{X'^1_b}\right)^\nu\right],$$

all t_ν being $t_\nu \geq 0$.

For $\delta = 0$, we get:

$$t_2 = \frac{1,875}{2} \left(\frac{2X^1_b}{R^2}\right)^2_{\epsilon=0.1} = 3,75 \cdot 10^{-2},$$

$\delta = 0.5$, we get:

$$t_2 = \frac{0.875}{2} \left(\frac{4X^1_b}{R^2}\right)^2_{\epsilon=0.1} = 7 \cdot 10^{-2}.$$

Eventually we get

$$q(X^1) = \frac{1+\alpha^2}{\alpha} \frac{T(X^1)}{p' R_\gamma R^2} \left[1 + \sum_{v=2,4,..} t_v \left(\frac{X^1}{X^1_b}\right)^\nu\right].$$

On the magnetic axis $X^1 = 0$, the exact result is

I.13 $$q(0) = \frac{1+\alpha^2}{\alpha} \frac{B_o}{p' R^2 \sqrt{1-\delta}}.$$

With $j_\phi = \sqrt{g_{22}}\, j^2$ and $e = \alpha/\sqrt{1-\delta}$, we can express q also in the following way:

$$q(0) = \frac{1+e^2}{e} \frac{B_o}{R \cdot j_\phi}.$$

The last equation shows how the values of e and j_ϕ can be varied for a constant q. Especially the current j_ϕ can be increased compared with the current in the circular cross section.

The ratio of kinetic pressure of the confined plasma and magnetic pressure of the toroidal magnetic field is

$$\beta_T = \frac{\int p \, d\tau}{1/2 \int (B_\phi)^2 \, d\tau} = \frac{\int p d\tau}{1/2 \int (T/r)^2 \, d\tau} \quad .$$

On the magnetic axis, we get

$$\beta_T(0) = \frac{1+\alpha^2}{q^2(0)} \epsilon^2 \frac{1}{1-\delta} \quad .$$

The exact β_T is:

$$\beta_T = \frac{1/2 \, \beta_T(0) \left[1+\frac{3}{8}\left(\frac{\epsilon}{1-\delta}\right)^2\right]}{(1+c'\epsilon^2)\left(1+\frac{\delta \beta_T(0)}{2(1+\alpha^2)}\right)} \qquad c' = 1+\frac{1}{2}\frac{1}{1-\delta}+\frac{3}{8}\left(\frac{1}{1-\delta}\right)^2 \quad .$$

With regard to the cases evaluated later on it is valid to set:

I.14 $$\beta_T \approx \frac{1}{2} \beta_T(0) = \frac{1+\alpha^2}{2q^2(0)} \epsilon^2 \frac{1}{1-\delta}$$

Accordingly we get a poloidal β_p for the poloidal magnetic field using the definition of Grad, Morgan [24]

I.15 $$\beta_p = \frac{\int p d\tau}{\int B_p^2 \, d\tau} \approx \frac{1+\alpha^2}{1+\alpha^2-\delta} = \frac{1+e^2(1-\delta)}{(1-\delta)(1+e^2)} \quad .$$

Diagram 1. Flux Surfaces ψ = constant, and Stagnation Points + of Equilibrium I.7.

a) $\alpha = 1,5$; $\delta = 0$

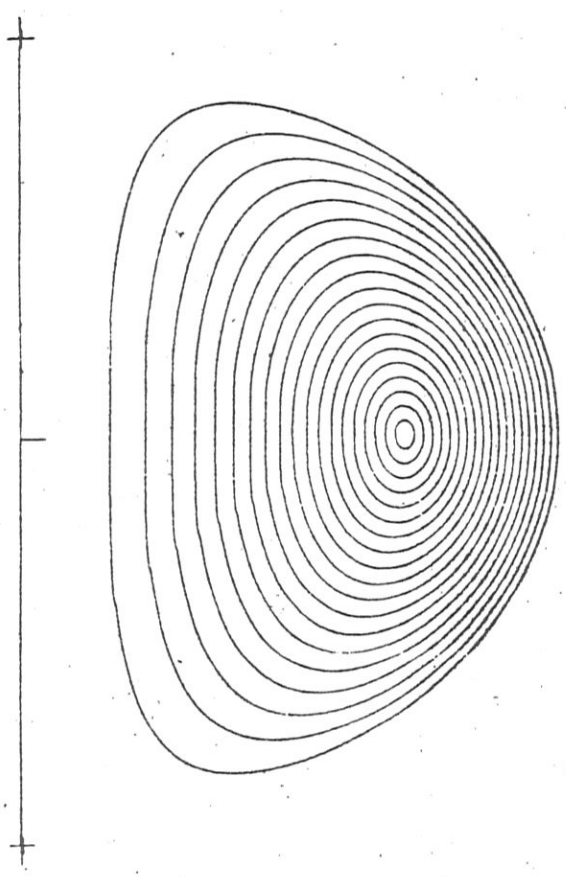

b) $\alpha = 1,5$; $\delta = 1/2$

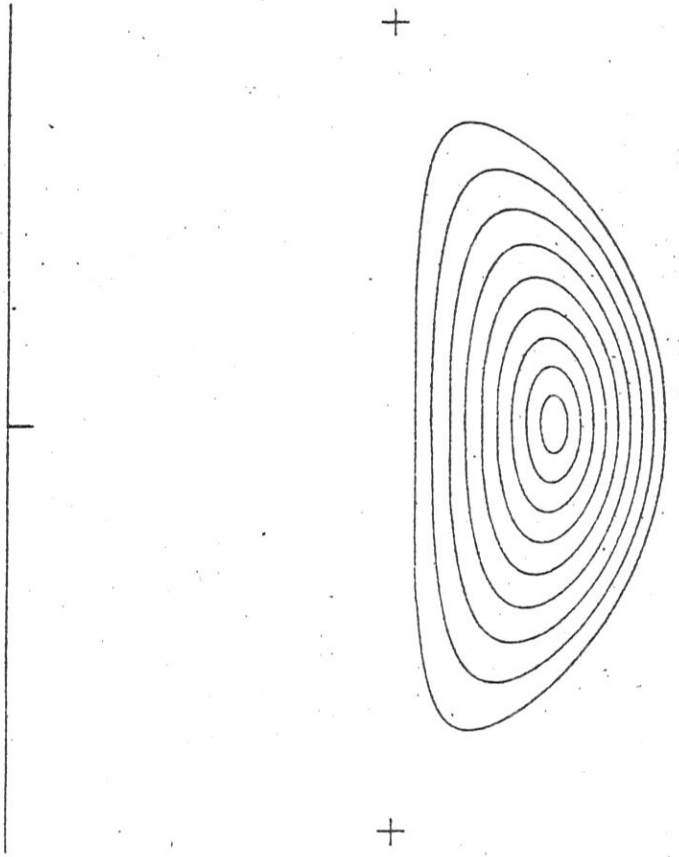

Diagram 2. Flux Surfaces ψ = constant, and Stagnation Points + of Equilibrium I.7.

a) $\alpha = 1,5$; $\delta = -1$

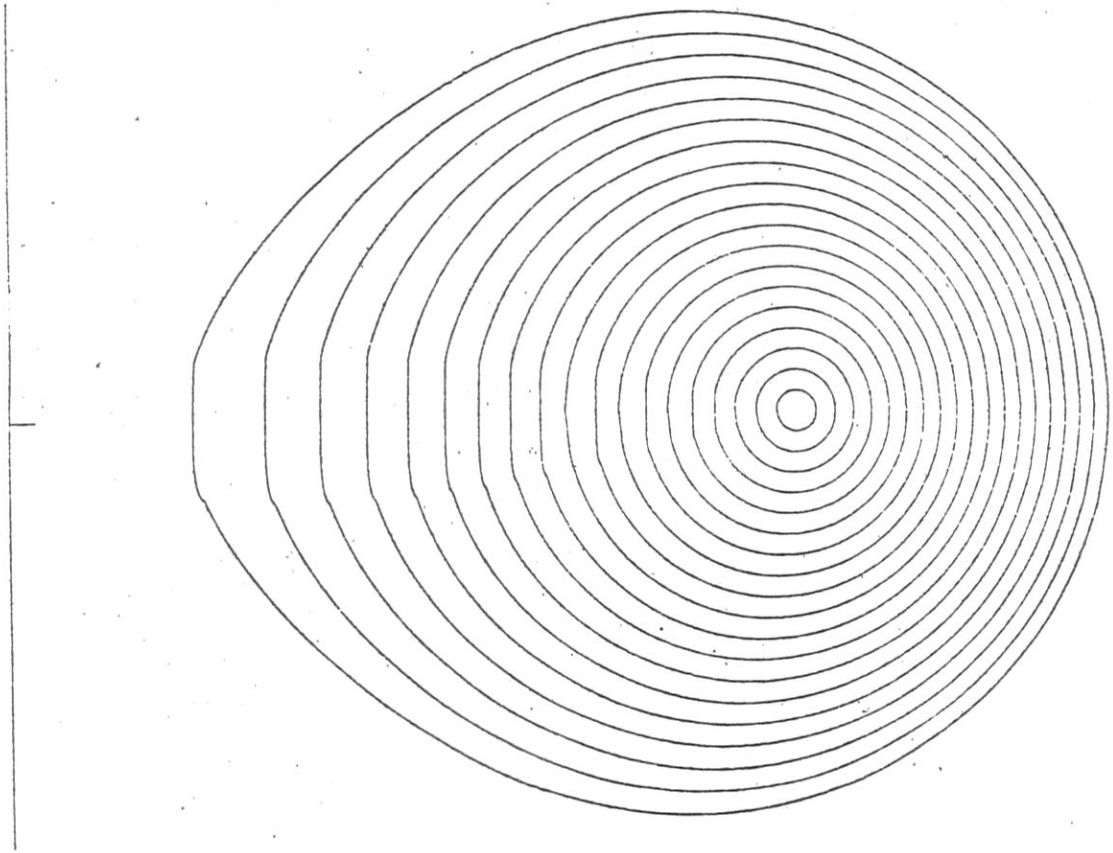

b) $\alpha = 5$; $\delta = -1$

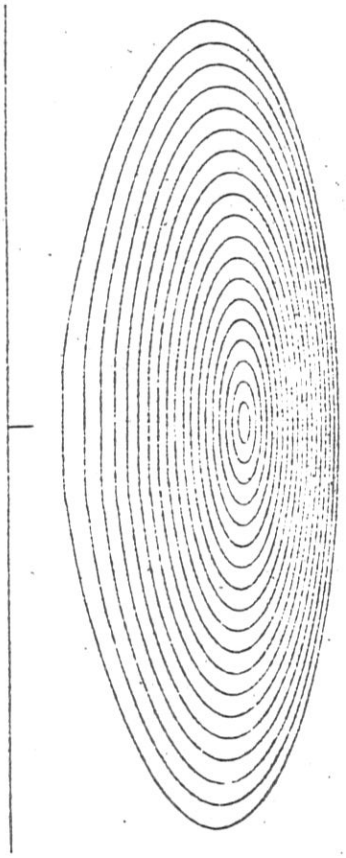

Diagram 3. Flux Surfaces ψ = constant, and Stagnation Points + of Equilibrium I.7.

a) $\alpha = 0,2$; $\delta = 0$

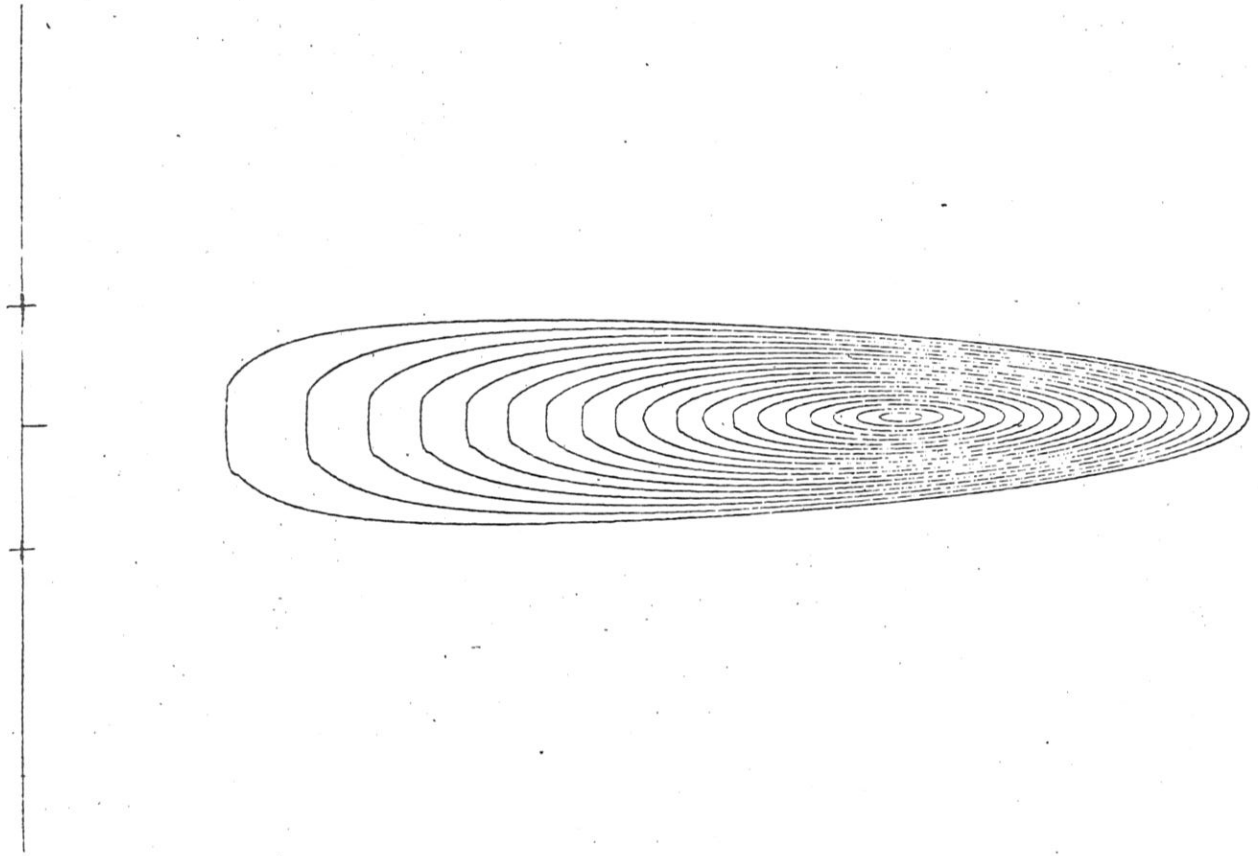

b) $\alpha = 5$; $\delta = 0$

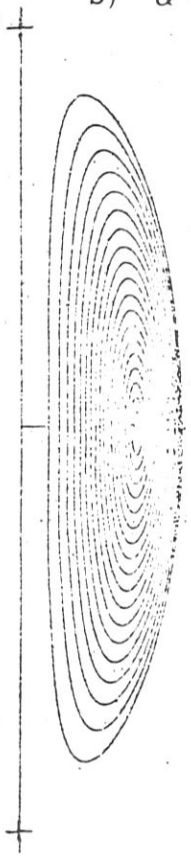

II. STABILITY

II.1 Energy Principle

In the linearized approximation of the MHD equations all perturbations of the equilibrium quantities in the plasma can be expressed by the displacement $\vec{\xi}(\vec{r},t)$ of the plasma and the perturbed magnetic field in vacuum $\delta\vec{B}_v$ by a vector potential $\vec{a}(\vec{r},t)$. The time dependence of the perturbations can be separated with an exponential function $e^{-i\omega t}$.

The energy integral for the plasma vacuum system consits of two parts. The contribution due to the surface integral vanishes since there is no surface current.

$$\delta W = \delta W_{PL} + \delta W_v \quad .$$

II.1 $$\delta W_{PL} = \frac{1}{2} \int_{\text{Plasma}} [\vec{Q}^2 + \vec{\xi}(\vec{Q}\times\vec{j}) + \nabla\cdot\vec{\xi}\,\vec{\xi}\cdot\nabla p + kp(\nabla\cdot\vec{\xi})^2]\, d\tau$$

II.2 $\vec{Q} = \nabla\times(\vec{\xi}\times\vec{B})$ denotes the magnetic field perturbation in the plasma

k is the ratio of specific heats

II.3 $$\delta W_v = \frac{1}{2} \int_{\text{vacuum}} (\delta\vec{B}_v)^2\, d\tau$$

II.4 $\delta\vec{B}_v = \nabla\times\vec{a}$ is the perturbation of the magnetic field in vacuum expressed by the vector potential $\vec{a}$.

According to the energy principle [2] and [3], test functions $\vec{\xi}(\vec{r})$ and $\vec{a}(\vec{r})$ which make δW negative are sufficient to prove instability if the following

boundary conditions are fulfilled:

II.5 $\vec{n} \times \vec{a} = -(\vec{n} \cdot \vec{\xi})\, \vec{B} = -\xi^1 \vec{B}$ at the plasma boundary

II.6 $\vec{n} \times \vec{a} = 0$ at the wall

$\vec{n}$ denotes the normal vector at the plasma boundary, resp. at the wall. For the wall situated at the plasma boundary the boundary condition is

II.7 $\vec{n} \cdot \vec{\xi} = 0,$

and the solution in the vacuum is $\delta \vec{B}_v = 0$.

The growth rates of the instabilities can be estimated to be [2] and [3]:

II.8 $|\omega^2| \geq |\omega_o^2| = -\frac{\delta W}{N}$; $\qquad N = \frac{1}{2} \int \rho \vec{\xi}^2 \, d\tau$.

For the proof of stability it is necessary to determine the minimum of δW with $\min(\delta W) \geq 0$.

II.2 Ansatz for the Test Functions

The minimization of δW is very difficult for the considered two-dimensional equilibrium. We do not try a complete minimization of δW with respect to $\vec{\xi}$ and $\vec{a}$ but use the eigenfunctions or approximated eigenfunctions of the corresponding cylindrical equilibria [4], [19] as an ansatz for the test functions in the toroidal system. With non-zero integers k (k, m being the wave numbers, the long and the short way round the torus) we have

$$\xi^i (X^1, X^2, X^3) = \sum_k \sum_m e^{ikX^2} e^{imX^3} \xi^i_{k,m} (X^1) ,$$

II.9

$$a_i (X^1, X^2, X^3) = \sum_k \sum_m e^{ikX^2} e^{imX^3} a_{i(k,m)} (X^1) .$$

Because of axisymmetry we can treat δW for each k separately. Alike to the solution of the straight system we take the real resp. imaginary part of the exponential functions. In addition we multiply this ansatz with a polynomial K_o in $u = (2X^1 / R^2) \cos X^3$ the relevance of which is shown in section II.3.

In the series II.9, we take the functions depending on X^1 only for one $m = \hat{m} \neq 0$ in analogy to the solution of the cylinder. Calculations with this Fourier component alone have indicated that the ansatz for the toroidal system cannot be improved further on.

We then take into account the components with $m = \hat{m} \pm 1$. It is shown by the qualitative investigation in section II.3 that for $m \neq \hat{m}$ the functions depending on X^1 are about one order of magnitude smaller than the corresponding ones for $m = \hat{m}$. We therefore assume the additional functions to be proportional to the corresponding one with $m = \hat{m}$. With respect to the boundary conditions we introduce for the plasma-vacuum system ten free constants and for the fixed boundary case six free constants. These constants are chosen in such a way that δW reaches its minimum value. We thus improve the ansatz for the test functions by minimization.

The stability calculation, however, is performed as general as possible. Then there exists the possibility to put in other or more Fourier components in II.9, and to use a more complicated minimization procedure in a following calculation.

Plasma

In the plasma we get with $k \neq 0$ for ξ^i:

$$\xi^1 = \sum_m f_m^1 (X^1) \cos(kX^2 + mX^3) \cdot K_o(u)$$

II.10

$$\xi^2 = \sum_m f_m^2 (X^1) \sin(kX^2 + mX^3) \cdot K_o(u)$$

$$\xi^3 = \sum_m f_m^3 (X^1) \sin(kX^2 + mX^3) \cdot K_o(u)$$

For $m = \hat{m} \neq 0$, the functions $f_m^i (X^1)$ are chosen in correspondence to the cylindrical case [4], [19] ($\beta = ct$).

$$f_m^1 = R \cdot k \left(\frac{1+\alpha^2}{2} \frac{1}{m^2\beta^2 - 1} \right)^{1/2} \left(\frac{m\beta - 1}{2m} J_{m+1}(y) + \frac{m\beta + 1}{2m} J_{m-1}(y) \right)$$

II.11

$$f_m^2 = k \frac{1+\alpha^2}{2} J_m(y) / m \cdot R$$

$$f_m^3 = R \cdot k \left(\frac{1+\alpha^2}{2} \frac{1}{m^2\beta^2 - 1} \right)^{1/2} \left(\frac{m\beta - 1}{2m} J_{m+1}(y) - \frac{m\beta + 1}{2m} J_{m-1}(y) \right)/X$$

$J_m(y)$ are Bessel functions with the argument

$$y = \left(\frac{1+\alpha^2}{2} \left(m^2 \beta^2 - 1 \right) \right)^{1/2} \frac{kX^1}{R^2}$$

$$\nabla \cdot \vec{\xi} = \frac{\partial_i (\sqrt{g}\, \xi^i)}{\sqrt{g}} = 0\,(\epsilon) \qquad \text{is of the order } \epsilon.$$

The plasma is not assumed to be incompressible in contrast to [4], [19]. With $Z = 1, 2$ and values of m_z in the interval (M_o, M_1) (M_o, M_1 being integers) we introduce

II.12 $\rho_z = k X^2 + m_z X^3$ and get with $\partial_p = \frac{\partial}{\partial X^p}$ from II.2:

II.2a $$Q^i_z = [\nabla \times (\vec{\xi}_z \times \vec{B})]^i = \epsilon^{ipq} \partial_p (\epsilon_{qmn} \xi^m_z B^n) .$$

ϵ^{ipg}, ϵ_{ipg} denote the contravariant and covariant components of the anti-symmetric ϵ tensor in curvilinear coordinates.

In the new coordinate system we get for δW_{PL} from Eq. II.1:

$$\delta W_{PL} = \frac{1}{2} \sum_{m_1, m_2 = M_o}^{M_1} \int_o^{X^1_b} dX^1 \int_o^{2\pi} dX^2 \int_o^{2\pi} dX^3 \sqrt{g} \Big[g_{ij} Q^i_1 Q^j_2$$

II.13

$$+ \xi^i_1 \epsilon_{ik\ell} Q^k_2 j^\ell + \frac{\partial_i (\sqrt{g}\, \xi^i_1)}{\sqrt{g}} \xi^j_2 \partial_j p$$

$$+ \frac{5}{3} p \left(\frac{\partial_i (\sqrt{g}\, \xi^i_1)}{\sqrt{g}} \right) \left(\frac{\partial_j (\sqrt{g}\, \xi^j_2)}{\sqrt{g}} \right) \Big] .$$

Indices occurring as subscripts and superscripts indicate summation from 1 to 3.

Analogously we get for the integral N in Eq. II.8:

$$\text{II.14} \qquad N = \frac{1}{2} \sum_{m_1, m_2 = M_o}^{M_1} \int_o^{X_b^1} dX^1 \int_o^{2\pi} dX^2 \int_o^{2\pi} dX^3 \sqrt{g} \, (g_{ij} \, \xi_1^i \, \xi_2^j)_\rho \, .$$

The density ρ is chosen as follows:

$$\text{II.15} \qquad \rho = \rho_o \left[1 - (X^1/X_b^1)^2\right]^{3/5} \qquad \rho_o = ct \, .$$

The outline shows the function ρ/ρ_o in dependence of X^1/X_b^1 .

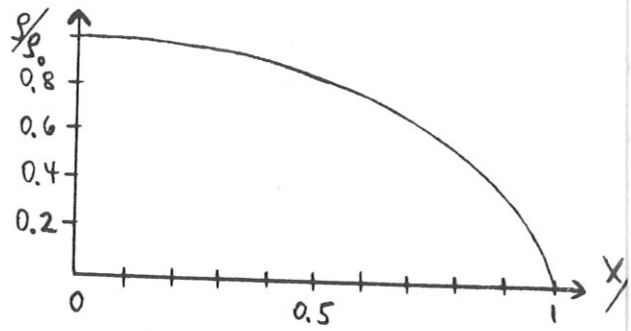

Vacuum

The covariant components of the vector potential $\vec{a}$ we choose in analogy to the straight system as follows [25] :

$$\text{II.16} \qquad \begin{aligned} a_1 \sqrt{g^{11}} &= a_r \\ a_2 \sqrt{g^{22}} &= a_z \\ a_3 \sqrt{g^{33}} &= a_\phi \end{aligned}$$

The solution for the cylinder is valid only for a circular cross-section $\alpha = 1$, $\delta = 0$. By introcuding a factor

$$C = \left(\frac{1 - \delta + \alpha^2}{2} \right)^{1/2} \frac{1}{\alpha}$$

which represents an average value of g_{11}, g_{33} with respect to X^3 and

$$y = \sqrt{\frac{1 + \alpha^2}{2}} \; \frac{kX^1}{R^2}$$

as the argument of the Bessel functions we get from II.16 with $\rho = kX^2 + mX^3$

$$a_1 = \frac{1}{R \cdot C} \left[C_1 K_{m-1}(y) - C_2 I_{m-1}(y) + \frac{B_1}{y} K_m(y) + \frac{B_2}{y} I_m(y) \right] K_o(u) \sin \rho ,$$

$$a_2 = -R \left[C_1 K_m(y) + C_2 I_m(y) \right] K_o(u) \cos \rho ,$$

$$a_3 = \frac{X^1}{R \cdot C} \left[C_1 K_{m-1}(y) - C_2 I_{m-1}(y) + \frac{B_1}{m} K'_m(y) + \frac{B_2}{m} I'_m(y) \right] K_o(u) \cos \rho .$$

I_n, K_n are modified Bessel functions, $'$ denotes the derivation with respect to the argument y. C_1, C_2, B_1, B_2 are constants. The boundary condition at the wall reads (II.6):

$$\epsilon^{ilk} a_k = 0 \qquad i = 1, 2, 3$$

From $a_2 = 0$ for $X^1 = X^1_w$ follows $\frac{C_2}{C_1} = -\frac{K^w_m}{I^w_m}$ and

from $a_3 = 0$ for $X^1 = X^1_w$ $\quad -B_2 = \frac{mC_1 (K^w_{m-1} - C_2/C_1 I^w_m) + B_1 K'^w_m}{I'^w_m}$.

The index w denotes the value of the function at the wall. Defining the functions

II.17 $$k_1 = K_{m-1}(y) - \frac{C_2}{C_1} I_{m-1}(y) - m \frac{(K^w_{m-1} - C_2/C_1 I^w_{m-1})}{I'^w_m} \frac{I_m(y)}{y}$$

$$k_2 = K_m(y) + \frac{C_2}{C_1} I_m(y)$$

$$k_3 = K_{m-1}(y) - \frac{C_2}{C_1} I_{m-1}(y) - \frac{(K^w_{m-1} - \frac{C_2}{C_1} I^w_{m-1}) I'_m(y)}{I'^w_m}$$

$$g_1 = \frac{K_m(y)}{y} - \frac{K'^w_m}{I'^w_m} \frac{I_m(y)}{y}$$

$$g_3 = \frac{1}{m} \left(K'_m(y) - \frac{K'^w_m}{I'^w_m} I'_m(y) \right)$$

we get

$$a_1 = \frac{1}{R \cdot C} \sin\rho \cdot K_o(u) (C_1 k_1 + B_1 g_1) ,$$

$$a_2 = - R \cos\rho \cdot K_o(u) C_1 k_2 ,$$

$$a_3 = \frac{X^1}{R \cdot C} \cos\rho \cdot K_o(u) (C_1 k_3 + B_1 g_3) .$$

The boundary condition at the plasma boundary reads (II.5):

$$\epsilon^{ilk} a_k = -\xi^1 B^i \qquad \text{for} \quad i = 1, 2, 3$$

$$a_2 = - \xi^1 B^3 \sqrt{g} \qquad \text{for} \quad X^1 = X^1_b .$$

This implies $C_1 = -\dfrac{\alpha X_b^1 f_b^1}{R k_2^b}\, CA$, with $CA = \dfrac{\alpha p'}{1+\alpha^2}$ the index b denoting the value of the functions at the plasma boundary. Furthermore, we have $a_3 = \xi^1 B^2 \sqrt{g}$ for $X^1 = X_b^1$ which implies

$$B_1 = \left(\frac{\alpha T(X_b^1)}{\hat{r}\, r^2}\, R \cdot C \cdot f_b^1 - C_1 k_b^3 \right) \frac{1}{g_3^b} \quad ,$$

$$\hat{r} = (r - \gamma)^{1/2} \quad .$$

Eventually we get the following ansatz for the vector potential for $m = \hat{m} \neq 0$:

$$a_1 = \alpha \cdot \sin\rho \cdot K_o(u) \left[- CA \cdot \phi_1 + \frac{T(X_b^1)}{r^2 \hat{r}}\, \Gamma_1 \right] \quad ,$$

II.18

$$a_2 = \alpha \cdot \cos\rho \cdot K_o(u)\, CA \cdot \phi_2 \quad ,$$

$$a_3 = \alpha \cdot \cos\rho \cdot K_o(u) \left[- CA\, \phi_3 + \frac{T(X_b^1)}{r^2 \hat{r}}\, \Gamma_3 \right] \quad ,$$

with the functions:

$$\phi_1 = \left(\frac{k_1^b}{k_2^b} - \frac{g_1 k_3^b}{k_2^b g_3^b} \right) \frac{X_b^1 \cdot f_b^1}{R^2 \cdot C}$$

II.19

$$\Gamma_1 = \frac{g_1^b}{g_3^b}\, f_b^1$$

$$\phi_2 = \frac{k_2^b}{k_2^b}\, X_b^1\, f_b^1$$

$$\phi_3 = \left(\frac{k_3^b}{k_2^b} - \frac{g_3 k_3^b}{k_2^b g_3^b} \right) \frac{X^1}{R^2 \cdot C}\, X_b^1\, f_b^1$$

$$\Gamma_3 = \frac{g_3}{g_3}\, f^1_b \cdot X^1 \ .$$

The general ansatz is according to Eq. II.9 given by summation over m with free functions for $m \neq \hat{m}$

$$\phi_{i(m)}(X^1) \ , \qquad \Gamma_{j(m)}(X^1) \ , \qquad i = 1,\ 2,\ 3 \qquad j = 1, 3$$

Then the vacuum integral reads (II.3, II.4):

$$\text{II.20} \quad \delta W_v = \frac{1}{2} \sum_{m_1, m_2 = M_o}^{M_1} \int_{X^1_b}^{X^1_w} dX^1 \int_o^{2\pi} dX^2 \int_o^{2\pi} dX^3 \sqrt{g} \left(g_{ij}\, \epsilon^{ik\ell}\, \partial_k a_{\ell(m_1)}\, \epsilon^{jk'\ell'}\, \partial_{k'} a_{\ell'(m_2)} \right) .$$

For the Fourier components $m = \hat{m} \pm 1$ in Eqs. II.10 and II.18, the functions depending on X^1 read:

$$f^i_m(X^1) = C^i_m \cdot f^i_{\hat{m}}(X^1) \qquad \text{for } i = 1,\ 2,\ 3$$

$$\text{II.21} \quad \phi_{1(m)}(X^1) = C^4_m \cdot \phi_{1(\hat{m})}(X^1)$$

$$\Gamma_{1(m)}(X^1) = C^5_m \cdot \Gamma_{1(\hat{m})}(X^1)$$

The functions $\phi_{2(m)}$, $\phi_{3(m)}$ and $\Gamma_{3(m)}$ have because of the boundary conditions the factor C^1_m .

Comment

In a similar way an ansatz for $\hat{m} = 0$ can be determined. Since then instabilities appear for values of q close to 0 this case is not evaluated. It is known that such perturbations can be stabilized.

Interesting, however, are perturbations with $k = 0$ and $\hat{m} \neq 0$ causing a shift of the whole plasma [26] . This case must be treated separatly, because the integration with respect to X^2 and X^3 in δW are different.

Description of displacement

The ξ^1 component is the most important part of $\vec{\xi}$. The physical component $\xi^{*1} = \xi^1 \sqrt{g_{11}}$ has the form (Eq. II.11 and I.9):

$$\xi^{*1} = K_o \cos (kX^2 + mX^3) f^1_m (X^1) \frac{\alpha}{R\sqrt{1-\delta}} \sqrt{\sin^2 X^3 + \frac{1-\delta}{\alpha^2} \cos^2 X^3} .$$

Neglecting the dependence on X^3 of K_o, i.e. $K_o \approx 1$, we set at the beginning $X^2 = 0$ and get for a fixed value of X^1:

$$\xi^{*1} = \frac{1}{R} \cos mX^3 \, H(X^3) = \frac{1}{R} \cos m X^3$$

$$e = 1$$

We examine $H(X^3) = \sqrt{(e^2-1) \sin^2 X^3 + 1}$ for $e < 1$ and $e > 1$.

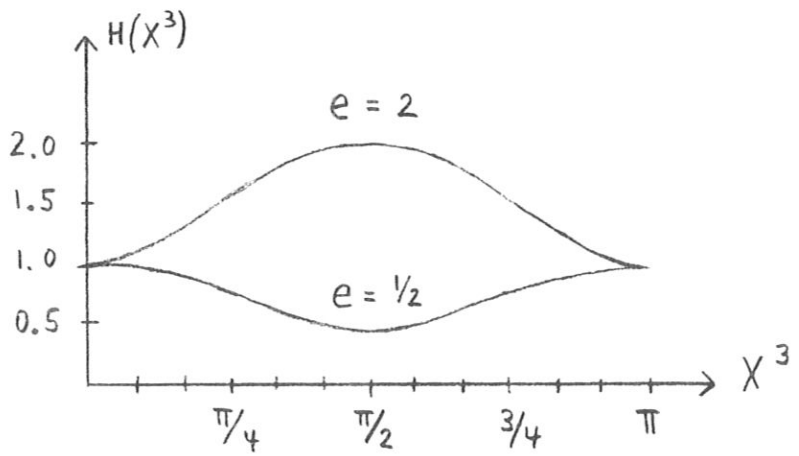

At the vertical half axes $X^3 = \pi/2,\ 3\pi/2$ the displacement ξ^{*1} is enlarged for $e > 1$ and reduced for $e < 1$.

e = 2

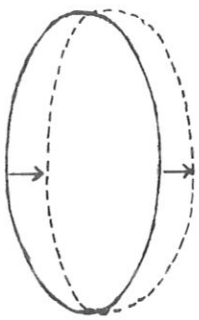

m = 1

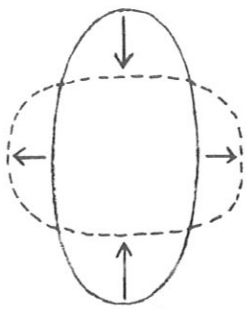

m = 2

e = 1/2

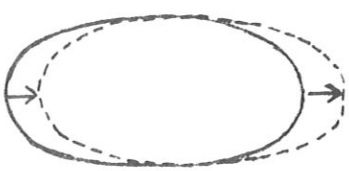

m = 1

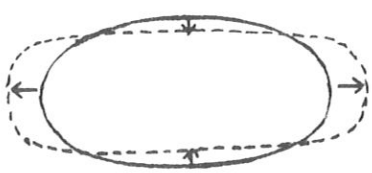

m = 2

With increasing values of X^2 these perturbations are shifted helically around the torus.

In nearly most cases the constants $C^1_{\hat{m}-1}$, $C^1_{\hat{m}+1}$ have values with $0.1 < C^1_{\hat{m}-1} < 0.6$ and $-0.6 < C^1_{\hat{m}+1} < -0.1$.

In the fixed boundary case these values are reduced by a factor 30 to 100.

II.3 Discussion of the Ansatz

We want to get a general view of the realization of instabilities. By that we are able to realize the significance of the polynomial $K_o(u)$ in Eq. II.10 and II.18 and to estimate the virtue of the ansatz. The influence of the toroidicity decreases with ϵ. However, we must not take ϵ alone as a measure, but only in connection with the magnitude of the growth rate. Instead of ω_o^2 in Eq. II.8 we discuss – as usual [4] –

$$\text{II. 22} \qquad Y_o^2 = \frac{\omega_o^2 \rho_o}{R^2 (1-\delta) CA^2} \qquad \text{with} \qquad CA = \frac{\alpha p'}{1+\alpha^2} \quad ,$$

being interpreted as a normalized growth rate. Y_o^2 represents the ratio of the velocity of the perturbation and the Alfven velocity with the poloidal magnetic field.

$$Y_o^2 \sim \frac{\omega_o^2 \rho_o (X^1/R)^2}{(B^{*3})^2} = \frac{\omega_o^2 L^2}{v_A^2} \quad ,$$

with $L = X^1/R$ being a radial length inside the plasma and $B^{*3} = B^3 \sqrt{g_{33}}$.

In the following discussion we have to separate the cases with free and fixed plasma boundary.

Free boundary

With one Fourier component $m = \hat{m}$ we get the magnetic field perturbation in the plasma from Eq. II.2 and II.2a with the indices c, s denoting the part proportional to $\cos\rho$ respectively $\sin\rho$ and $CE = \gamma\ (\alpha p'/1+\alpha^2)^2$, $K_1(u) = \frac{\partial}{\partial u} K_o(u)$:

$$Q^{1,s} = -f^1_m K_o(u)\, CA\, \tilde{r} k\, (q - m/k)$$

II.23
$$Q^{1,c} = +f^1_m K_1(u)\, CA\, \tilde{r} \cdot \frac{2X^1}{R^2} \cdot \sin X^3$$

$$Q^{2,s} = -CA\, \tilde{r}\, X^1 \sin X^3 \left(\frac{q}{r^2} f^3_m (2 + r^2/\tilde{r}^2) K_o - \frac{K_1}{R^2} (2q f^3_m + 2 f^2_m) \right)$$

$$Q^{2,c} = -CA\, \tilde{r} \left(-k \cdot f^2_m \cdot K_o \cdot (q - m/k) - \frac{q}{r^2} f^1_m (2 + r^2/\tilde{r}^2) K_o \cos X^3 \right.$$

$$\left. + K_1/R^2\, 2q \cos X^3 f^1_m + CE \frac{X^1 f^1_m}{q r^4 \tilde{r}^2 CA^2} \cdot K_o \right)$$

$$Q^{3,s} = 0$$

$$Q^{3,c} = CA\, \tilde{r} \left(k f^3_m K_o (q - m/k) + \frac{2}{R^2} \cos X^3 K_1 f^1_m \right) .$$

The terms of order $\theta(\epsilon)$ in $(\nabla \cdot \vec{\xi})^2$ and $\xi \cdot \nabla p\ \nabla \cdot \vec{\xi}$ also contributing to δW are not given, since they partly cancel each other and since their influence is small first of all for small ϵ.

Using the following relations:

$$\phi_2 + \frac{k}{m}\phi_3 = \Gamma_3$$

$$\partial_1\phi_2 + k\phi_1 = m\Gamma_1$$

$$m\Gamma_1 - \partial_1\Gamma_3 = -k\left(\frac{1}{m}\,\partial_1\phi_3 - \phi_1\right)$$

we get for the perturbation of the magnetic field in vacuum from Eq. II.4

$$\delta B_v^{1,s} = -CA\,\tilde{r}\,\frac{k\Gamma_3}{X^1}\cdot\left(q - \frac{m}{k}\right)\cdot K_o$$

$$\delta B_v^{1,c} = CA\,\tilde{r}\,\frac{2\sin X^3}{R^2}\,\phi_2\cdot K_1$$

II.24

$$\delta B_v^{2,v} = CA\,\tilde{r}\sin X^3\left[\frac{2}{R^2}\,\phi_1 K_1 + \frac{q}{r^2}\,\Gamma_1\left(2 + \frac{r^2}{\tilde{r}^2}\right)K_o - \frac{2q}{R^2}\,\Gamma_1\cdot K_1\right]$$

$$\delta B_v^{2,c} = CA\,\tilde{r}\left[-\frac{k}{m}\left(\partial_1\phi_3 - \phi_1\right)\frac{1}{X^1}\left(q - \frac{m}{k}\right)K_o + \frac{q}{r^2}\cos X^3\left(2 + \frac{r^2}{\tilde{r}^2}\right)\right.$$

$$\left.\cdot\,\Gamma_3 K_o - \frac{2}{R^2}\cos X^3\, q K_1\Gamma_3\right]$$

$$B_v^{3,s} = 0$$

$$B_v^{3,c} = -CA\,\tilde{r}\left[m\cdot\frac{k}{m}\cdot\frac{\Gamma_1}{X^1}\left(q - \frac{m}{k}\right)\cdot K_o - \frac{2\cos X^3}{R^2}\,\frac{\phi_2}{X^1}\cdot K_1\right] .$$

Instabilities occur in the cylinder if

$$m - \frac{2}{m\beta} \leq kq \leq m .$$

The constant β is determined by the boundary conditions.

Generally, we have

$$\frac{2}{m\beta} = 1 - (X_b^1 / X_w^1)^{2m} \qquad \text{if} \quad X_b^1 / X_w^1 \neq 1 .$$

For the elliptical case there are similar relations [5] and [19] .

The quantity $y = kq - m$ has values with $|y| < \frac{2}{m\beta}$ in most cases $|y| < 1$*. This means that the perturbations follow approximately the field lines. $\vec{Q}^2$ and $\delta \vec{B}_v^2$ are proportional to y^2. The current term in δW being proportional to y can predominate and gives δW a negative value. The maximum value of Y_o^2 is given by $\max (Y_o^2) = (1/m\beta)^2$.

In the toroidal system, we find the cylindrical terms again which are underlined in Eq. II.23, II.24 . The additional contributions resulting from derivatives of the expression $(1/r^2 \tilde{r})(\sim B^2 \sqrt{g})$ may have large values. We demonstrate this fact with $Q^{2,c} \sqrt{g_{22}}$ containing the following expression

$$r \cdot \frac{q}{r^2} \cdot f_m^1 \left(2 + \frac{r^2}{\hat{r}^2}\right) K_o \cos X^3 \underset{\delta=0}{\approx} 3q (f_m^1)_{Zyl} \cdot \underset{K_o = 1}{K_o} = 3q (f_m^1)_{Zyl} .$$

This expression does not become small if ϵ goes to zero. The polynomial $K_o(u)$ is defined in such a way that these inconvenient terms are compensated. We make with

---

* For m different from $\hat{m}$ the value of $|y|$ is not small. In order that δW can have negative values, the functions $\xi^i_{(m)}(X^1)$ and $a_{i(m)}(X^1)$ in II.9 have to be an order of magnitude smaller than the corresponding ones $\xi^i_{(\hat{m})}$, $a_{i(\hat{m})}$.

II.25 $K_o = 1 + d_1 u + d_2 u^2$ with

$$d_1 = \frac{1}{2}\left(2 + \frac{1}{1-\delta}\right) \underset{\delta=0}{=} 1,5$$

$$d_2 = \frac{1}{1-\delta}\,\frac{d_1}{4} \underset{\delta=0}{=} \frac{d_1}{4}$$

these terms proportional to ϵ^2 .

This holds for all components of the perturbed toroidal magnetic fields in plasma and vacuum.

The toroidal contributions to δW still remaining are proportional to $t_z = 2X^1/R^2 \cdot \cos X^3$, $2X^1/R^2 \cdot \sin X^3$ or X^1/R^2, we take into account the g_{ij} and the constants R within the definitions of f^i_m, ϕ_i, Γ_j. At the plasma boundary it holds that $t_z \sim 2\epsilon$, and the wall $t_z \sim 4\epsilon$. Thereby the vacuum interval is especially enlarged.

If the stabilizing wall has a great distance from the plasma, this being valid for $X^1_w = 2X^1_b$, the dependence of the constant β and therefore of the normalized growth rate y^2_o on ϵ is weak. We have to compare t_z with $|y|$ at the point of the strongest instability, i.e., for $|y| = 1/2$.

The requirement that the toroidal terms are small reads

II.26 $$t_z = 4\epsilon \frac{1}{1-\delta} < 1/2 \ .$$

Our ansatz will give good results, if Eq. II.26 is fulfilled, i.e., (1) for an inverse aspect ratio ϵ smaller than $1/8$ with $\delta = 0$, (2) for small ϵ and negative values of δ.

Inconvenient in view of this ansatz are an enlargement of ϵ, a positive value for δ and a reduction of the distance of the wall to the plasma.

Fixed boundary

For the fixed boundary case Y_o^2 is very small. For example, for $\epsilon = 1/10$ and $k = 1$, $\hat{m} = 1$ we have $\beta \simeq 37$ resulting in $\max(Y_o^2) \simeq 10^{-3}$. With decreasing ϵ the value of β becomes even greater so that the growth rate decreases further on and the toroidal effects predominate.

The instabilities arise here in a more complicated way than in the free boundary case. The boundary condition $f_m^1(X_b^1) = 0$ (Eq. II.7) implies that $f_m^3(X^1)$ changes the sign for a fixed $X^1 = X_o^1$ and thereby also the current term being proportional to $f_m^1 \cdot f_m^3$. The current term, therefore, consists of two contributions which almost cancel each other. It is possible, that small toroidal contributions result in remarkable changes of the current term. With the given test functions the stability behavior of the toroidal system may be different from that of the cylinder. Only for very small values of q instabilities can be expected surely, since then the growth rates in the cylinder are strong.

II.4 Computational Program

The evaluation of the perturbed magnetic fields Q^i (Eq. II.2a) and δB_v^i (Eq. II.4) and later on of the integrands of δW_{PL} (Eq. II.13), N (Eq. II.14) and δW_v (Eq. II.20) can be carried out analytically. The expressions, however, are very extensive. The integration with respect to X^2 in δW and N

can be performed analytically, while the integration with respect to X^3 results in elliptical integrals because of the functions

$$r = R\left(1+\frac{2X^1}{R^2}\cdot\cos X^3\right)^{1/2},$$

$$\tilde{r} = R\sqrt{1-\delta}\left(1+2\frac{X^1}{R^2(1-\delta)}\cos X^3\right)^{1/2},$$

and products therefrom. In order to avoid these elliptical integrals we expand such functions into Taylor series. It is known that the expansion of $\tilde{r}^i r^j$ is absolute convergent for real i,j and [27]

$$|2X^1/R^2|, \quad |2X^1/R^2(1-\delta)| < 1.$$

The remainder is arbitrary small if sufficient many terms are taken into account. Thus, the integration with respect to X^3 can be performed analytically with an error being arbitrary small.

The last integration with respect to X^1 is done numerically because of the Bessel functions in II.11, II.17, and II.19. By this procedure it is possible to evaluate δW and N with a very high accuracy.

The minimization of δW with respect to the constants C_m^i (Eq. II.21) leads to a linear, inhomogeneous system of equations which is solved numerically. Thus, we get a partition of the computational program into an algebraic and a numerical part.

Since the algebraic expressions are very lengthy, the algebra is done by computer using the language REDUCE . The algebraic program contains the freedom to truncate the Taylor series at a arbitrary high order. In addition

the number Fourier components is variable. The algebraic calculation is described in detail in [21]. Thereby, in this procedure a check is made to ensure that the Taylor series are truncated at a sufficiently high order so that the result is not influenced by the remainders.

We are able to chose all parameters of the equilibrium freely, especially ϵ. The virtue of our stability calculation is given by the virtue of the ansatz, but not by an approximation within the procedure.

The numerical program (FORTRAN) contains the evaluation of algorithm determined by the algebraic program, i.e., evaluation of "operators" introduced there [21]. In order to reach a high accuracy we separate the positive and negative parts contributing to δW, i.e., $\delta W = \delta W_+ - \delta W_-$ with $\delta W_\pm \geq 0$, so that cancellations can occur only once. Thereby we get an estimate about the accuracy required in every part of the program. There are cancelled 3 to 7 digits (in very few cases 9 digits). The FORTRAN program uses double precision including the evaluation of the Bessel function [31] and the solving of the system of equations [30]. The numerical integration is done with 128 grid points.

The Taylor series are truncated beyond the 12th to 21st term depending on the i, j of $\hat{r}^i r^j$. These integers $N = N(i,j)$ are determined by the requirement that for a aspect ratio $\epsilon^{-1} = 10$ the remainder has a absolute value smaller than 10^{-6}. With decreasing ϵ^{-1}, N is increased.

The procedure gives the value of the normalized growth rate Y_o^2 accurate to two digits at least.

Computing Time

The computing time for the complete symbolic manipulation with REDUCE 2 is 40 minutes. This represents a third of the computing time required in [6], although ten times this figure was first estimated. The storage requirement for the symbolic manipulation is 720 K bytes.

The computing time for a set of parameters in the numerical program (FORTRAN) with three Fourier components for the test functions, including minimization, is:

(a) with vacuum 20 s,

(b) without vacuum 10 s.

In this case, too, distinct optimization has been achieved relative to the program in [6], which requires about twice these times. For a small aspect ratio $\epsilon^{-1} \approx 6$ the computing times increase to (a) 30 s, and (b) 15 s, owing to the continued Taylor expansion.

The storage requirement for the complete numerical program is 180 K bytes (compared with 720 K bytes in the separate programs for δW_{PL} and δW_{V} in [6]).

III. RESULTS

In representing the results of the stability calculations we distinguish between the two cases of a free plasma boundary and a fixed plasma boundary.

The instabilities occurring are represented by the normalized growth rate Y_o^2 from Eq.(II.22) as a function of the safety factor $q = q(0)$ on the magnetic axis from Eq. (I.13), and the results are discussed for various values of the aspect ratio ϵ^{-1}. All cases are calculated with three Fourier components for the test functions (with $m = \hat{m}$, $\hat{m} \pm 1$) and with the given minimization of δW.

From Y_o^2 we obtain for the growth rate ω_o^2 in Eq. (II.8):

III.1 $$\omega_o^2 = Y_o^2 \frac{p_o}{\rho_o L_o^2} \frac{2(1-\delta)}{1+\alpha^2}$$

with the plasma radius $L_o = X_b^1/R$. p_o and ρ_o denote the pressure and mass density respectively on the magnetic axis. Thus, $Y_o^2 = 1$ with a plasma pressure $p_o = 10^5$ dyne/cm^2, a plasma density $\rho_o = 10^{-10}$ g cm^{-3}, and a plasma radius $L_o = 31$ cm corresponds to a growth rate in the microsecond range:

$$\omega_o = 10^{+6} \sqrt{\frac{2(1-\delta)}{1+\alpha^2}} \ \text{s}^{-1} .$$

$\Lambda = X_w^1/X_b^1$ is the ratio of the wall radius to the plasma radius and indicates how far the stabilizing wall is from the plasma boundary.

Free Plasma Boundary

(a) Aspect ratio $\epsilon^{-1} \approx 20$

For aspect ratios of 20 and higher and with a distinct wall, i.e., $\Lambda > 1.5$, there is excellent agreement between the stability behavior of the torus and cylinder. This agreement is used for the circular plasma cross section ($\alpha = 1$ and $\delta = 0$) to check the computer program. The results of Küppers, Pfirsch, and Tasso are [6] thus confirmed and, since the class of test functions is larger, extended.

As Figs. 7-9 show, with $\Lambda = 2$ and $\delta = 0$, we find instabilities for lying and standing ellipses as plasma boundary with ratios of half axes between 0.1 and 10 for values of q between 0 and 8.

At $\alpha > 4$ instabilities are still obtained for $q > 8$. In general, configurations with standing ellipses as boundary curves are unstable in a larger region for q.

The widening of the instability regimes given by Laval et al. and Dewar et al. [5], which is particularly pronounced for large ellipticity, is not found. For $k = 1$ and $\hat{m} = 1, 2, 3, \ldots$, however, the entire range of values of q, except for very small regions around integral values, is already covered with instabilities.

The corresponding instabilities with $k = 2, 3$ which restrict these stable q ranges even more are not given here, but they do exist.

We are particularly interested in the stabilizing effect of the wall. Figures 7-9 therefore show the instabilities for various Λ values with $1 < \Lambda \leq 2$. It can be seen that perturbations with large $\hat{m}$ values are less

stabilized by the wall than those with low values. This stabilization consists in widening the stability islands, but is really only effective for $\Lambda < 1.1$. For $1 < \Lambda < 1.1$ we no longer find at $k = 2, 3$ the corresponding instabilities, and so in the context of the perturbations possible here stability islands do in fact occur for $q \gtrsim v$ ($v = 1, 2, 3, \ldots$), preferably for large $v \geq 2$.

For a paramagnetic poloidal current, i.e., $\delta < 0$, we find roughly the same instabilities. This case is not discussed further here.

For a diamagnetic poloidal current, i.e., $\delta > 0$ (Fig. 10), it is only for $\delta \geq 3/4$ that we find fewer instabilities, preferably for small values of α, which according to Eq.[I.15] with $\alpha = 0.1$ ($e = 0.2$) means a poloidal $\beta_p \approx 4$, and with $\alpha = 1/2$ ($e = 1$) a $\beta_p \approx 2$. The value of β_T is increased by a factor of 4. According to the estimate [II.26], however, our ansatz is not adopted to such values of δ, probably because an overestimation of the vacuum term δW_v. Tayler [4], on the other hand, gives stabilization (for a cylindrical equilibrium with surface current) when the current distribution is paramagnetic. The same applies in our calculation for the case where the stabilizing wall is immediately at the plasma boundary.

An increase of α also causes an increase of β_T, but then more instabilities occur.

The largest value of q for which instabilities are still found is used to calculate the corresponding value of β_T according to Eq. [I.14]. These critical β_T values represent an upper bound of the β_T ensuring stability. Stability islands are, of course, not taken into account here. Figure 4 shows these critical β_T (as β_T/ϵ^2) as a function of the axis ratio e[I.12].

(b) Aspect ratio $\epsilon^{-1} \approx 10$

With a distant wall, i.e., $\Lambda = 2$, we find instabilities for values of q with $0 < q < 6$, $k = 1, 2,$ and $\hat{m} = 1, 2, 3, 4$. The stabilizing influence of the wall is shown in Fig. 11.

The influence of a paramagnetic or diamagnetic, poloidal current is shown in Figs. 12 and 13. It can be seen that our ansatz is particularly suitable for the paramagnetic case. Instabilities are found here, preferably for small values of α, i.e., for lying ellipses as flux surfaces in the vicinity of the magnetic axis. The critical β_T as a function of e is shown in Fig. 4.

Diagram 4. The Critical β_T/ϵ^2 as a Function of the Ratio of Halfaxes e.

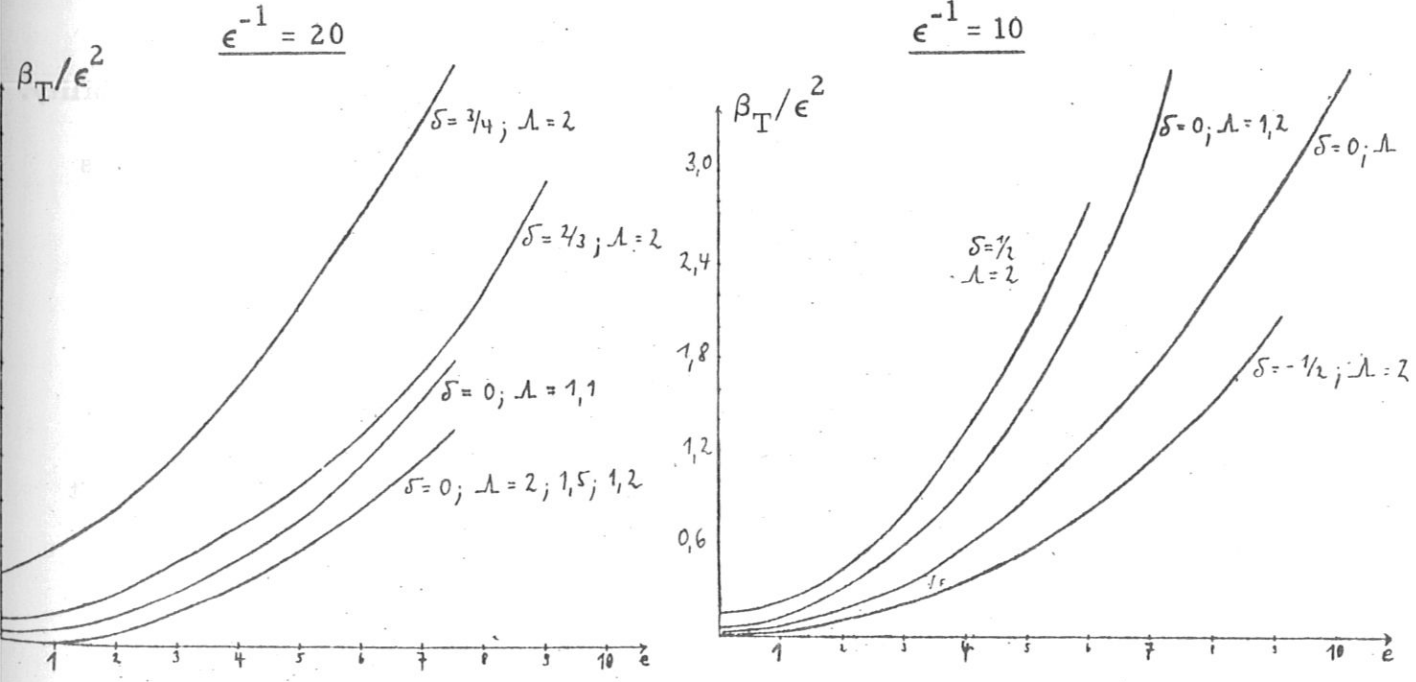

(c) Aspect ratio $\epsilon^{-1} \approx 8$

For an aspect ratio of 8 and smaller the test functions of the cylinder are no longer sufficient alone. In order to detect instabilities in the torus, we need the minimization procedure, which may yield completely different perturbations. Figure 14 shows the instabilities for q between 0 and 3 with k = 1, 2.

The instabilities for a paramagnetic current distribution with $0 < q < 5$ are shown in Fig. 15. It is again seen that the cases with small α values yield the most instabilities. This makes it clear how well the eigenfunctions of the problem have to be approximated.

The calculations with diamagnetic current distributions $\delta = 1/2$, yield no significant instabilities.

(d) Aspect ratio $\epsilon^{-1} \approx 6$

These cases represent, for the time being, the limit of our stability calculation. Here the absence of instabilities may not be interpreted as stability. Our method, however, yields with sufficient numerical accuracy instabilities for values of q between zero and 4, as Figs. 16 and 17 show.

Fixed Plasma Boundary

The conducting wall is located directly at the plasma boundary. The boundary condition $f_r^1 (X_b^1) = 0$ fixes the constant β from Eq. II.11. The most important result is that fewer instabilities occur in this case than in the corresponding cylindrical equilibria. This agrees with the qualitative estimates in Sec. II.3. With the wall immediately at the plasma boundary stabilization

Diagram 5. The Critical β_T/ϵ^2 as a Function of the Ratio of Halfaxes e.

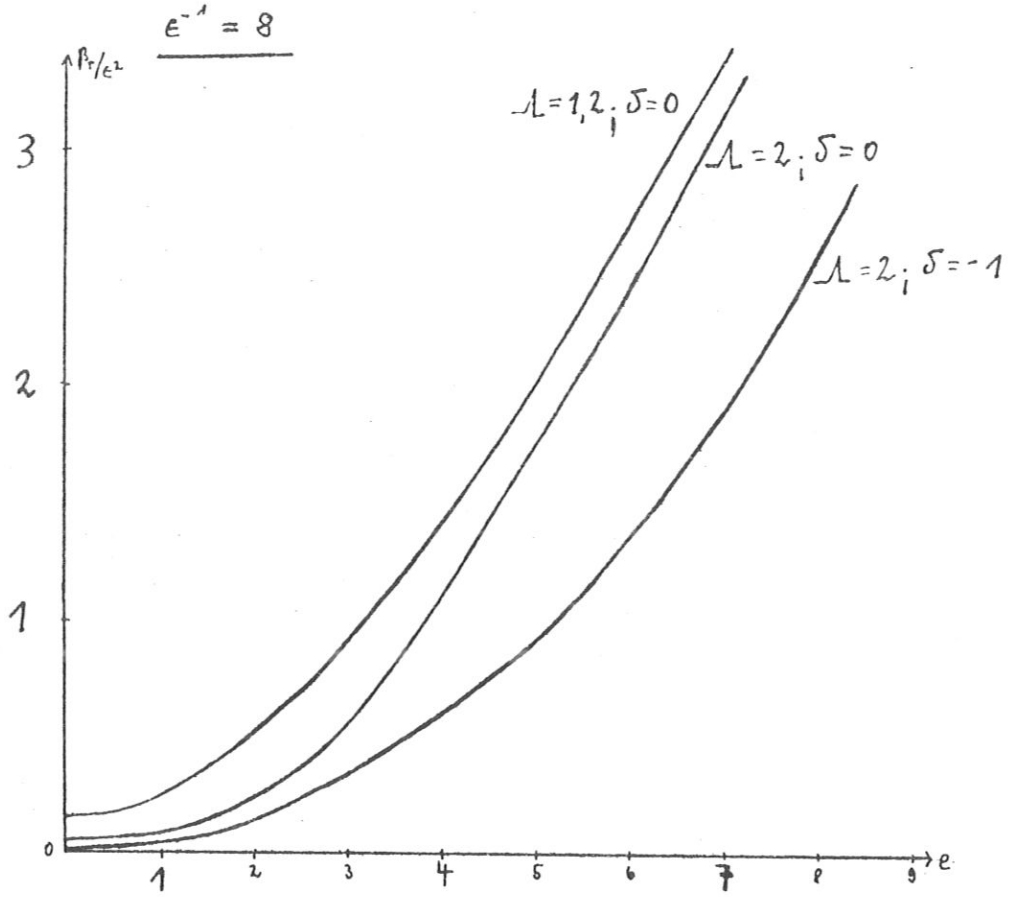

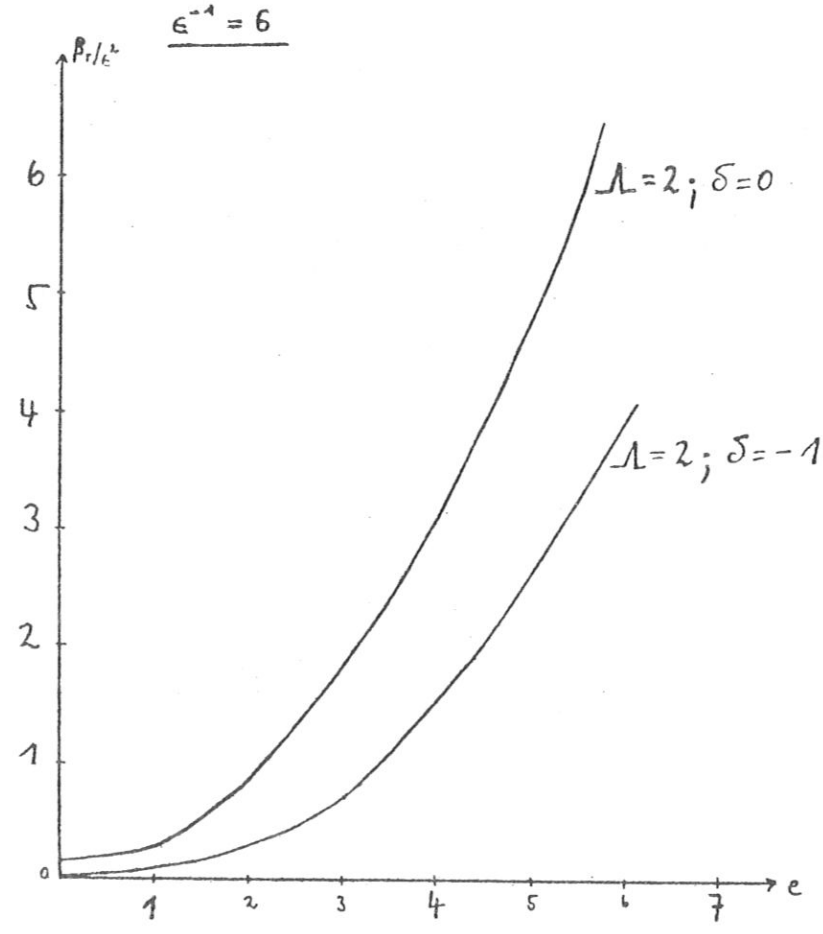

is extremely effective because instabilities are only found for values of q smaller than 2 (with $\alpha \leq 6$ even only for $q < 0.7$).

We make the calculations with k, $\hat{m} = 1, 2, 3, 4, 5, 6$ for an aspect ratio between 3 and 40. The most pronounced instabilities are found for an aspect ratio between 6 and 8. A paramagnetic current distribution ($\delta < 0$) has a slightly stabilizing effect, while a diamagnetic distribution is destabilizing in the context of our perturbations. In the circular case $\alpha = 1$, $\delta = 0$ instabilities are only found for values of q smaller than 0.25. For highly elliptic flux surfaces $\alpha = 17, 20$ instabilities exist up to $q \leq 2$, and hence for q larger than unity. Y_0^2 with $\alpha \leq 4$ is about two orders of magnitude smaller than for perturbations which change the plasma boundary. The growth rate ω_o thus decreases by an order of magnitude. For large α values, $\alpha > 4$, small aspect ratio $\epsilon^{-1} \leq 8$ and a diamagnetic current distribution $\delta > 0$ Y_0^2 asummes a value of almost unity in each case and is then roughly just as large as in the free boundary case.

The results are compatible with Lortz's sufficient criterion for stability [11], [12]. In regions where the necessary Mercier criterion for localized perturbations is satisfied [6], [12] there are no instabilities either.

Figures 18-21 show the instabilities for an aspect ratio with $4 \leq \epsilon^{-1} \leq 20$. For the critical β_T/ϵ^2 as a function of α (Fig. 6) we obtain in almost all cases investigated an almost constant value:

$$\beta_T/\epsilon^2 \approx 25/1 - \delta \qquad \text{for} \quad \delta \geq 0 \quad \text{and} \quad \epsilon^{-1} \geq 6$$

$$\beta_T/\epsilon^2 \approx 25 \qquad \text{for} \quad \delta < 0 .$$

Owing to the finite conductivity σ of the metal wall the perturbed magnetic field can penetrate to a depth d:

$$d \sim \sqrt{1/\sigma\omega_o} \quad .$$

In most experiments the discharge time is longer than the time taken by the perturbations to penetrate the wall, The conducting wall then no longer has any stabilizing influence. A wall with finite resistence cannot produce complete stabilization but at most damping of the growth rates, as is shown in [17] .

Diagram 6. Critical β_T/ϵ^2 as a Function of $\alpha = e\sqrt{1-\delta}$ for a Fixed Plasma Boundary .

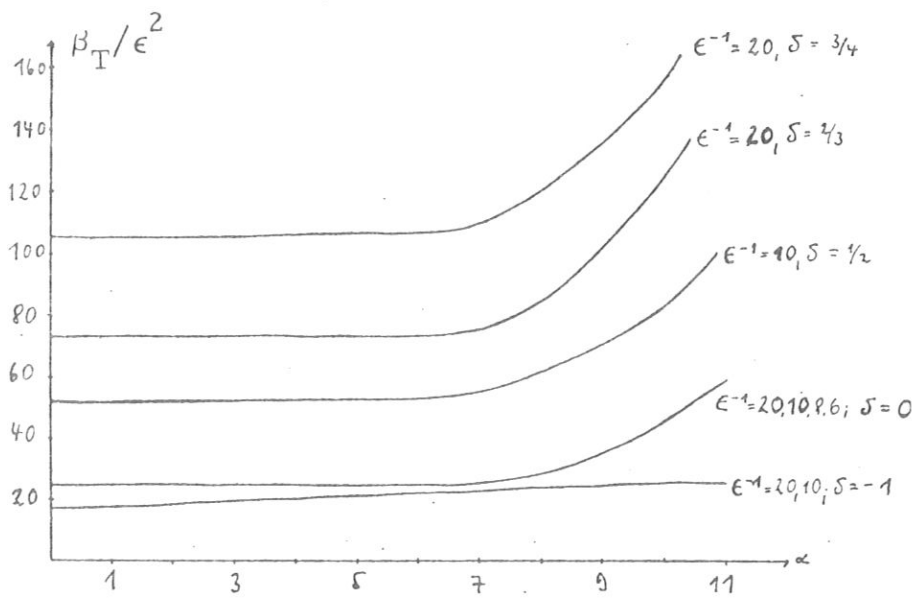

Discussion of Results

With a free plasma boundary there are instabilities below and above the Kruskal-Shafranov limit. This result is valid for every aspect ratio investigated, i.e., for $\epsilon^{-1} > 5$.

With an aspect ratio larger than 10 and with the wall far from the plasma ($\Lambda > 1.5$) the stability behavior of the torus and cylinder are the same if the poloidal current is not too high. In general, equilibria with highly elliptic cross sections are more unstable than those with circular cross sections. With standing ellipses this is particularly valid for diamagnetic current distributions and for lying ellipses particularly for paramagnetic current distributions. As the cylindrical solution is only exact in the circular case, it is to be assumed that the test functions are more favorable for the circle than for ellipses with large ellipticity. More instabilities are therefore expected particularly for ellipses.

The wall only has a strongly stabilizing effect if it is in the immediate vicinity of the plasma boundary. According to our calculations stabilization with a decreasing aspect ratio is already effective at larger distances. It is also possible, however, that our ansatz is not favorable for these cases, probably owing to an overestimation of the vacuum integral, and so an improvement in the test functions may yield new instabilities.

Stabilization with the wall immediately at the plasma boundary is particularly pronounced for equilibria with a ratio of half axes of the cross sectional areas smaller than 4 since instabilities only occur here for values of

q smaller than 0.7, and at the same time the growth rate ω_o is reduced by at least one order of magnitude relative to the free boundary. By comparison, standing ellipses with a larger axis ratio are more unfavorable.

The belt pinch for our equilibria is characterized by an aspect ratio of 10, an axis ratio of 10, and only a small poloidal current. For a fixed value of q such an equilibrium has a high beta $\beta_T \sim e^2$ and a high toroidal current $j_\phi \sim e$. But, the stability behavior is more infavorable owing to the increase in instabilities and poor wall stabilization. The growth rates are in the microwave range $\omega_o \sim (1-10) \cdot 10^5 \ s^{-1}$.

We can summarize that for this class of instabilities the favorable equilibria are given by the parameters $0.8 < \alpha < 3$; $\delta > 0$; $\Lambda \leq 1.2$; $q \geq 3$, and $\epsilon^{-1} \leq 8$. These are equilibria with diamagnetic current distributions, slightly D-shaped cross sections with ratio of half axes between 1 and 3, and small wall-to-plasma distances. In this case the critical $\beta_T/\epsilon^2 \approx 0.1 - 1$.

For JET (Joint European Torus) it is planned to have an aspect ratio of 2.5 and a D-shaped cross section with an axis ratio of 1.7. Our results are only valid for JET if it is assumed that the stability behavior is approximately the same for $\epsilon^{-1} = 2.5$ to $\epsilon^{-1} = 8$, which some experiments suggest. This equilibrium is then favorable in our sense, but this, of course, does not mean complete stability.

In our calculation strong instabilities are given by $Y_o^2 \sim 1$, and weak ones by $Y_o^2 \sim 10^{-2}$. For the experiments, however, growth rates in the millisecond range are still dangerous, which means $Y_o^2 \sim 10^{-6}$. Whether such

marginal values can be calculated with sufficient accuracy seems questionable since a cancellation in δW of 7 to 12 places has to be expected and since, on the other hand, the cancellation and the rounding error are increased owing to the many Fourier components necessary. This should also be true for other stability calculations.

In our calculation the numerical accuracy according to Sec. II.4, and [21] is very good. A calculation with 5 or 7 Fourier components is, therefore, also possible. The calculation presented here will be extended using a more general set of global expansion functions and an improved minimization procedure.

In order to allow a stability calculation for numerically determined equilibria, the equilibrium solution has, in our experience, to have a relative exactness of 10^{-5} to 10^{-9}.

SUMMARY

The stability of tokamak equilibria with volume current has hitherto been investigated only approximately. The critical points involved are:

(1) Validity of the surface current model.

(2) Restriction to perturbations with fixed plasma boundary.

(3) Validity of the expansion with respect to the inverse aspect ratio.

In an exact calculation without these restrictive assumptions we show that MHD instabilities occur in the tokamak equilibria investigated. The stability investigation is made by means of the energy principle using test functions. In this method the stability limit remains undetermined. The exact tokamak equilibria investigated have an almost constant volume current in the toroidal direction and, in addition, a poloidal current which generates a diamagnetic or paramagnetic current distribution. The plasma cross sections are ellipse-like with arbitrary axis ratios. The plasma pressure decreases outward. The plasma is surrounded by a vacuum extending to a perfectly conducting wall. The ansatz for the test functions is derived from the eigenfunctions of the corresponding cylindrical equilibria and suitably modified. The perturbations essentially consist of three coupled modes in the cylinder [4] . The strength of the coupling is determinated in such a way that δW assumes its minimum value.

The extensive algebraic calculations are done by computer using the REDUCE programming language. All parameters of the equilibrium solution can be arbitrarily varied. Evaluation is mainly for aspect ratios larger than 5, axis ratios of the cross sectional areas between 0.1 and 10 and values of

the safety factor between 0 and 8. The wall-to-plasma distance is thereby varied. The normalized growth rate of the instabilities is plotted as a function of the safety factor q. The growth rates of the unstable perturbations are in the microsecond range. With a free plasma boundary there are instabilities below and above the Kruskal-Shafranov limit for every aspect ratio investigated (i.e., $\epsilon^{-1} > 5$). In general, there are more instabilities in equilibria with strongly elliptic cross sections than in those with circular cross sections. For an aspect ratio larger than 10 and with the wall far away the stability behavior of the torus and cylinder are the same if the poloidal current is not too high. A small aspect ratio and a highly diamagnetic current distribution have a stabilizing effect on perturbations which change the plasma boundary. This, however, does not mean that such equilibria are stable, because improvement of the test functions can yield new instabilities.

If the wall is located immediately at the plasma boundary, the instabilities found are compatible with the sufficient criterion for stability formulated by Lortz [12].

The instabilities determined yield a "critical" ($\hat{\beta}_T$) which represents an upper bound of the β_T values permissible for stability. The equilibria that are favorable in the context of these investigations have a

$$\hat{\beta}_T / \epsilon^2 \simeq 0.1 - 1 .$$

ACKNOWLEDGMENTS

I wish to thank Professor Dr. D. Pfirsch and Dr. H. Tasso for stimulating the theme of this work and for interesting and helpful discussions. I am indepted to Mr. J. Steuerwald for his help concerning all problems of programming. Further, I want to thank Mrs. M. Weissenburger (PPPL) for her careful typing of the manuscript.

REFERENCES

[1] K. Hain, R. Lüst, and A. Schlüter
Z. f. Naturforschung 12a, 833 (1957).

[2] I. B. Bernstein et al.,
Proc. Roy. Soc. (London) A 244, 17 (1958).

[3] G. Laval, C. Mercier, and R. Pellat
Nucl. Fusion 5, 156 (1965).

[4] R. J. Tayler,
Proc. Phys. Soc. (London) B 70, 1049 (1957).

[5] G. Laval, R. Pellat, and J. L. Soule
Phys. Fluids 17, 835 (1974).

R. L. Dewar, et al., Phys. Fluids 17, 930 (1974).

[6] G. Küppers, D. Pfirsch, and H. Tasso
Proc. of the IAEA Conf. on Plasma Physics and Controlled Nuclear Fusion Research, Madison, Wisconsin, (1971).

[7] E. Martensen and K. V. Sengbusch
Proc. of the Eleventh International Congress of Applied Mechanics, Munich (1964) pp. 1010-1013.

[8] J. P. Freidberg and F. A. Haas
Phys. Fluids 16, 1909 (1973).

[9] B. M. Marder
Phys. Fluids 17, 634 (1974).

[10] E. A. Frieman, et al.,
Princeton Plasma Physics Laboratory Report no. MATT-942 (1972).

[11] D. Lortz
Nucl. Fusion 13, 817 (1973).

[12] D. Lortz and J. Nührenberg
Nucl.Fusion 13, 821 (1973).

[13] J. P. Freidberg and B. M. Marder
Phys. Fluids 16, no. 2, 249 (1973).

[14] D. A. Baker and L. W. Mann
Proc. of the Second Topical Conference on Pulsed High-Beta Plasma
Garching, July 3-6, 1972, W. Lotz, Ed., IPP 1/127, Vol. 7, p. 69.

[15] G. Bateman, W. Grossman, and W. Schneider
Garching Report IPP 1/145, April 1974.

[16] K. v. Hagenow and K. Lackner
Equilibrium Calculations for JET , JET Workshop, February 13, 1974
Paper no. A.2.

[17] D. Pfirsch and H. Tasso
Nucl. Fusion 11, 259 (1971).

[18] D. Pfirsch and H. Tasso
Comments Plasma Physics 1, 139 (1972).

[19] W. Kerner
unpublished

[20] M. D. Kruskal, J. L. Johnson, M. B. Gottlieb, and L. M. Goldman
Phys. Fluids 1, 421 (1958);

V. D. Shafranov
Plasma Physics and the Problem of Controlled Thermonuclear Reactions
M. A. Leontovich, Ed. (Pergamon, New York, 1959) Vol. II, p. 197.

[21] W. Kerner and J. Steuerwald
Institute for Plasma Physics, Garching Report no. 6/123 (1974).

[22] E. Klingbeil
Tensorrechnung für Ingenieure, B. I. Hochschultaschenbücher,
Bd. 197/197a.

[23] W. Kerner, D. Pfirsch, and H. Tasso
Nucl, Fusion 12, 433 (1972).

[24] H. Grad and J. Morgan
Phys. Rev. Letters 24, 1337 (1970).

[25] H. Tasso
Private communication.

[26] P. H. Rutherford
Princeton Plasma Physics Laboratory Report MATT-976 (1973).

[27] E. Martensen
Analysis I Par. 27, B. I. Hochschultaschenbücher, Band 832.

[28] A. C. Hearn
REDUCE 2 User's Manual, Stanford Artificial Intelligence Project
Mmo - No AIM-133 (1970).

[29] A. C. Hearn
Application of Symbolic Manipulation in Theoretical Physics
University of Utah, Contract-Nr. F 30602-70-C-0300.

[30] GAUNIT: Programm aus der Benutzerprogrammbibliothek des IPP
(H. Pillsticker).

[31] BESSEL: Programm aus der Benutzerprogrammbibliothek des IPP
(G. Hocke, H. Pillsticker)

Diagram 7. The Normalized Growth Rate Y_o^2 as a Function of the Safety Factor q for Aspect Ratio $\epsilon^{-1} = 20$ without Poloidal Current ($\delta = 0$).

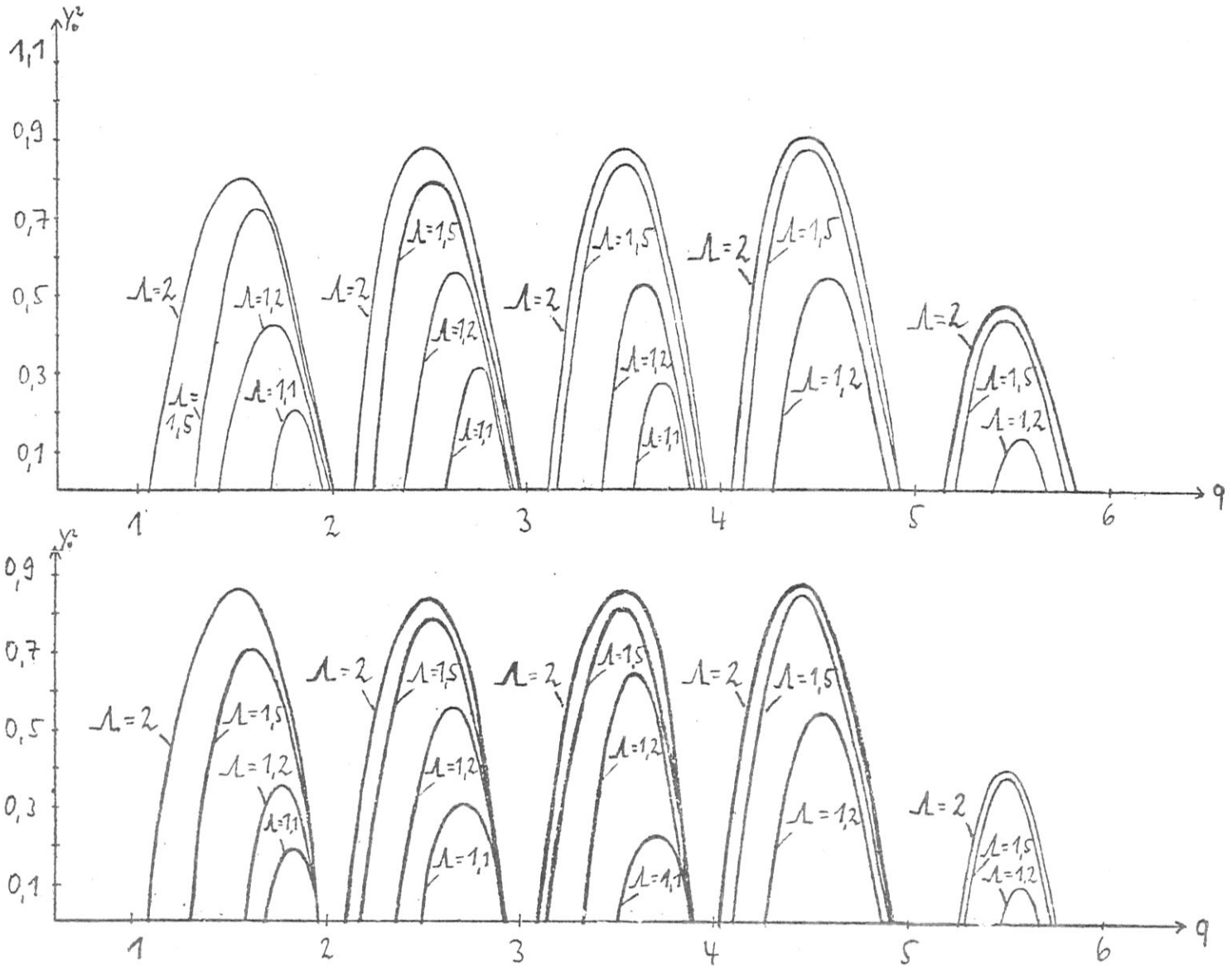

Diagram 8. The Normalized Growth Rate Y_o^2 as a Function of the Safety Factor q for Aspect Ratio $\epsilon^{-1} = 20$ without Poloidal Current ($\delta = 0$).

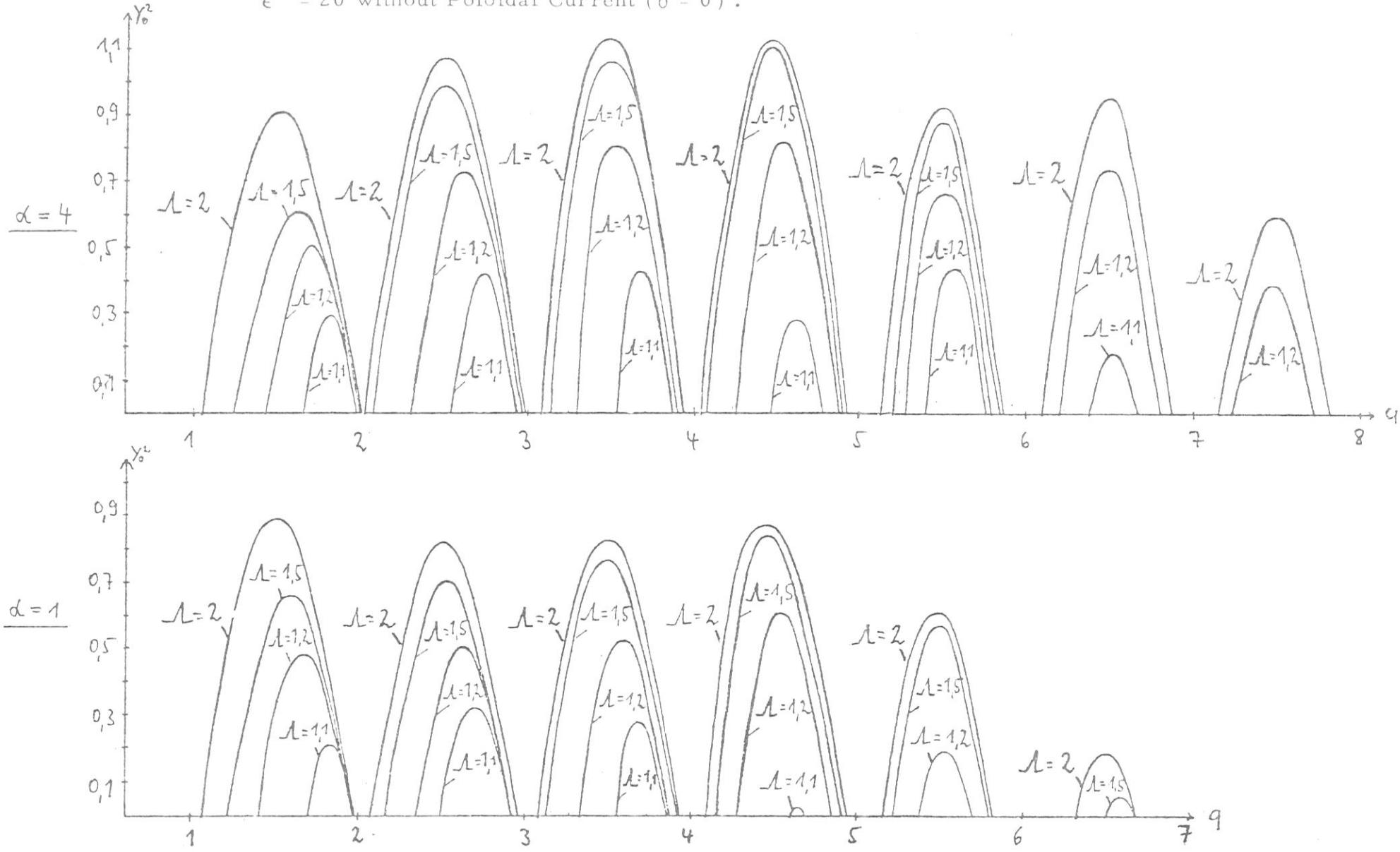

$\epsilon^{-1} = 20$ without Poloidal Current ($\delta = 0$) .

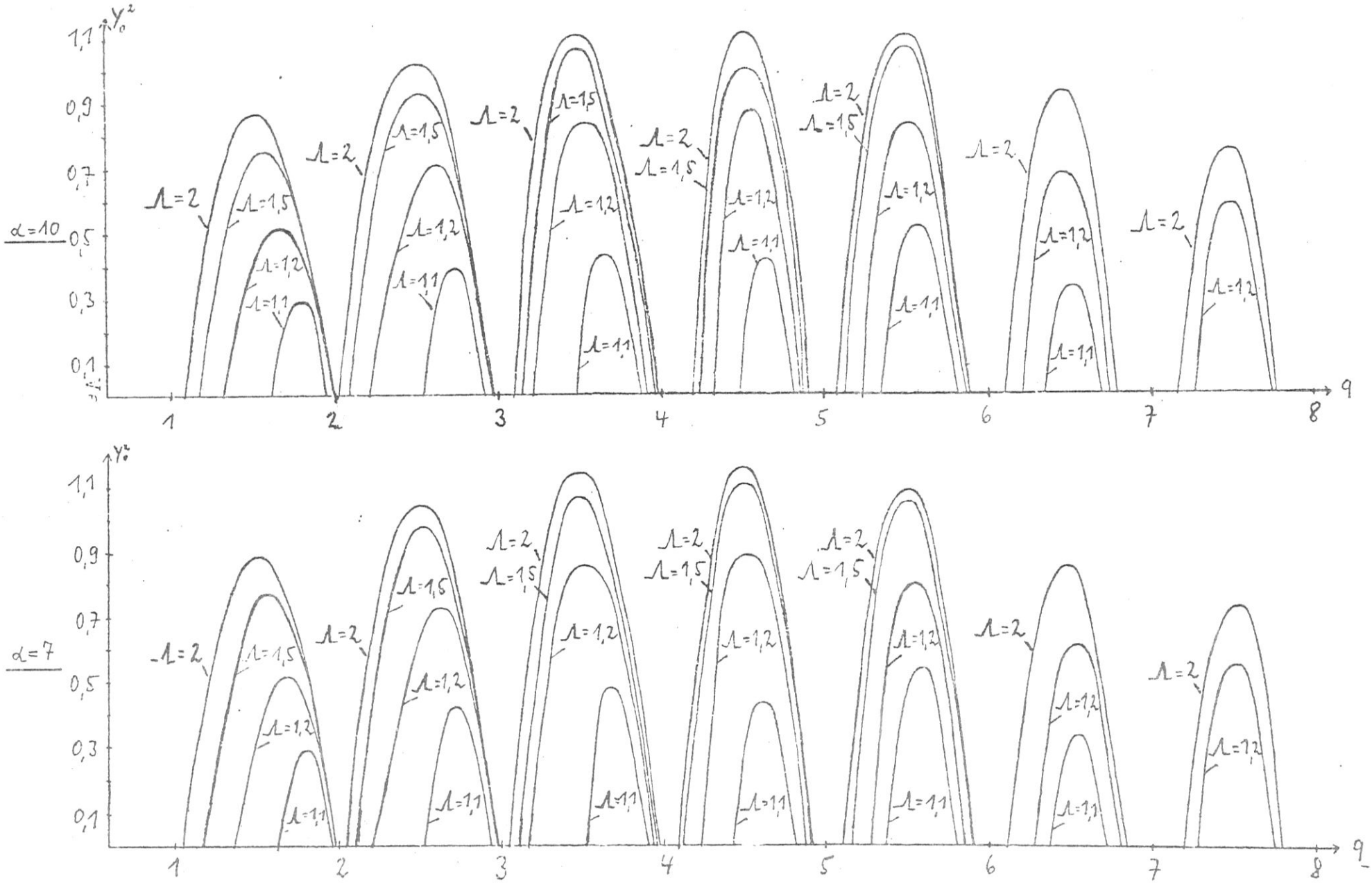

Diagram 10. The Normalized Growth Rate Y_o^2 as a Function of the Safety Factor q $\epsilon^{-1} = 20$, $\Lambda = 2$, — $\delta = 2/3$, --- $\delta = 3/4$.

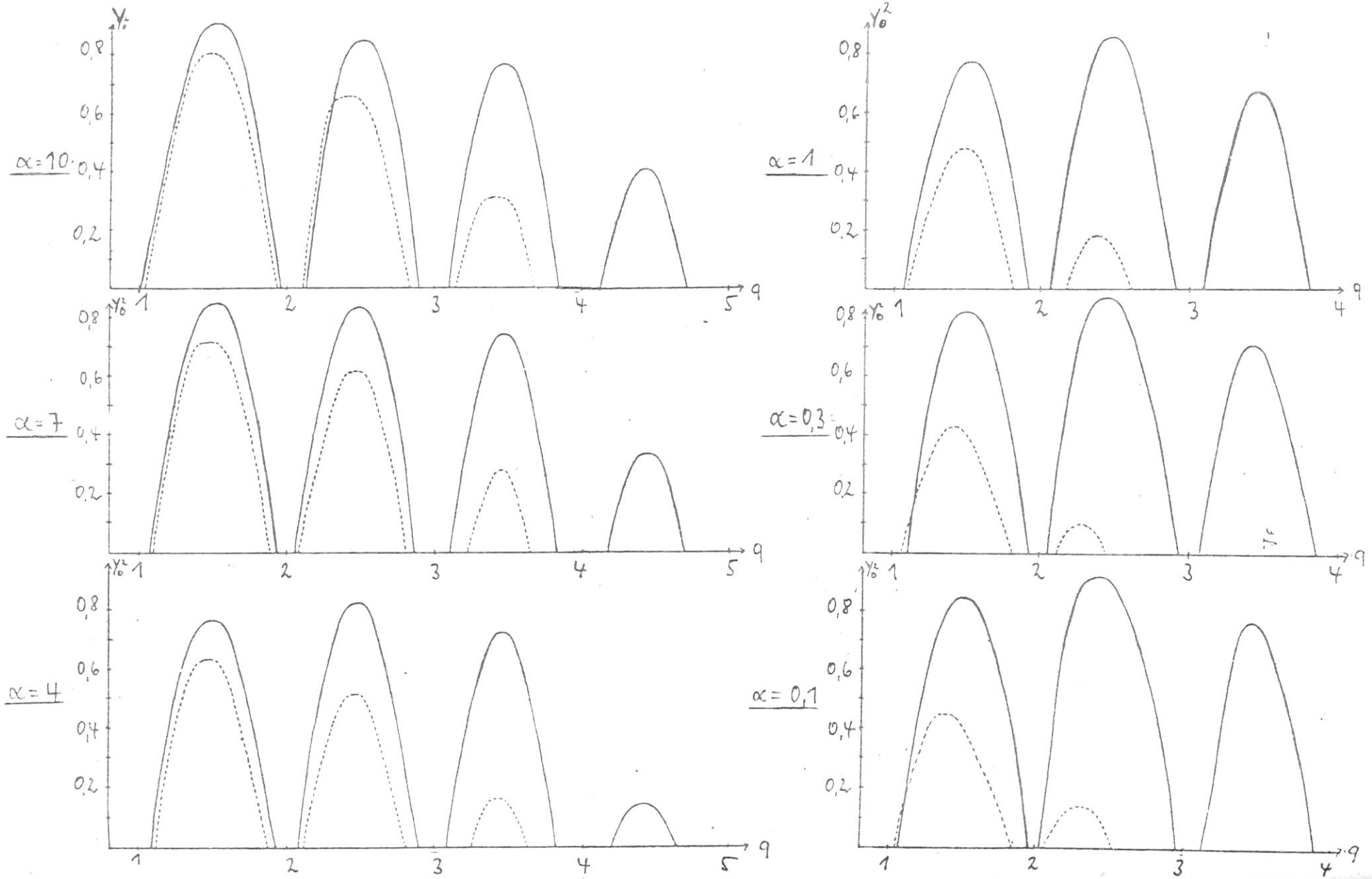

Diagram II. The Normalized Growth Rate as a Function of the Safety Factor q, $\varepsilon = 10$, $\delta = 0$,
– $\Lambda = 2$, --- $\Lambda = 1, 2$.

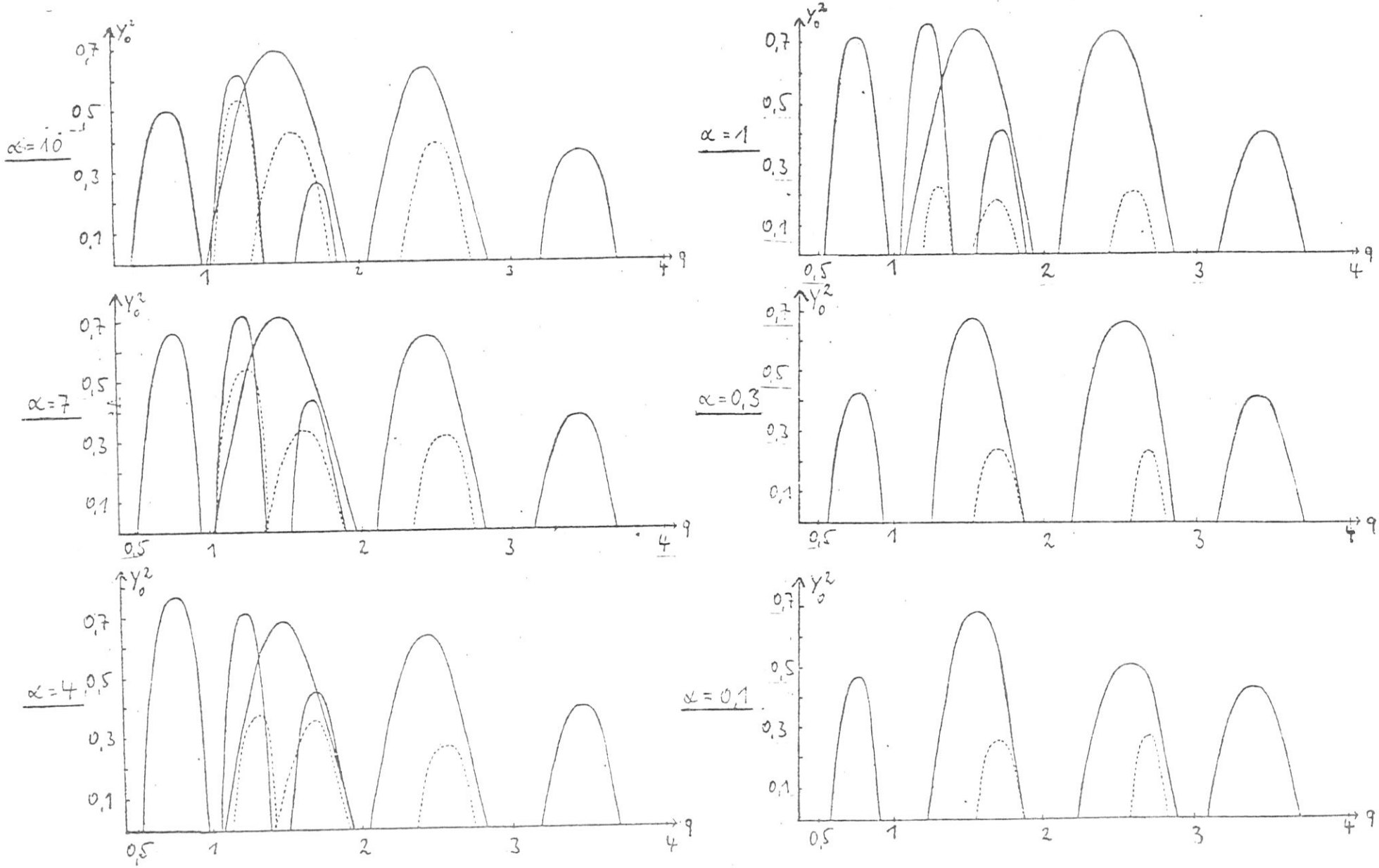

Diagram 12 . The Normalized Growth Rate as a Function of the Safety Factor q, for Aspect Ratio $\epsilon^{-1} = 10$ with Poloidal Current; $\Lambda = 2$.

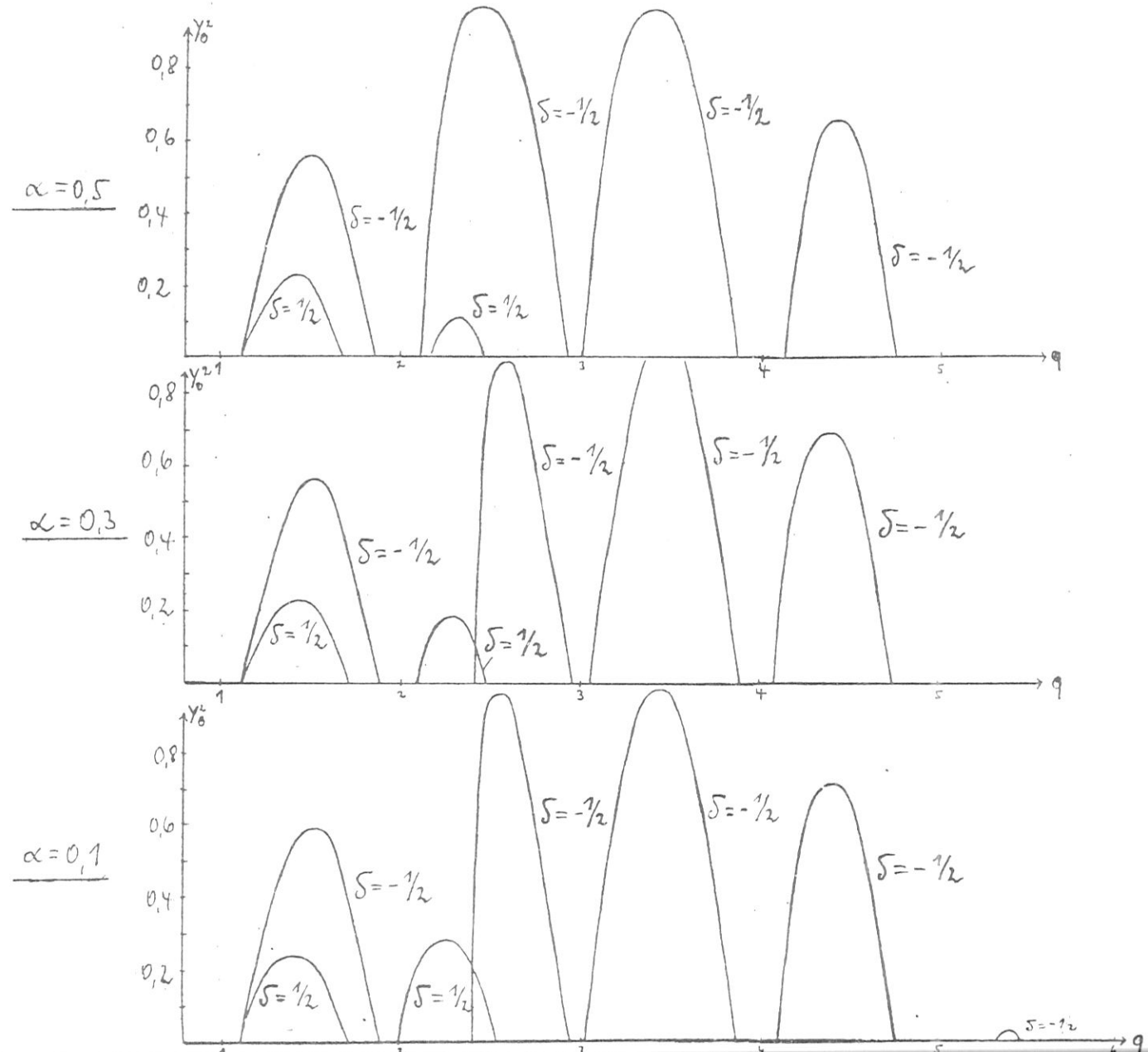

Diagram 13. The Normalized Growth Rate as a Function of the Safety Factor q for Aspect Ratio $\epsilon^{-1} = 10$ with Poloidal Current; $\Lambda = 2$.

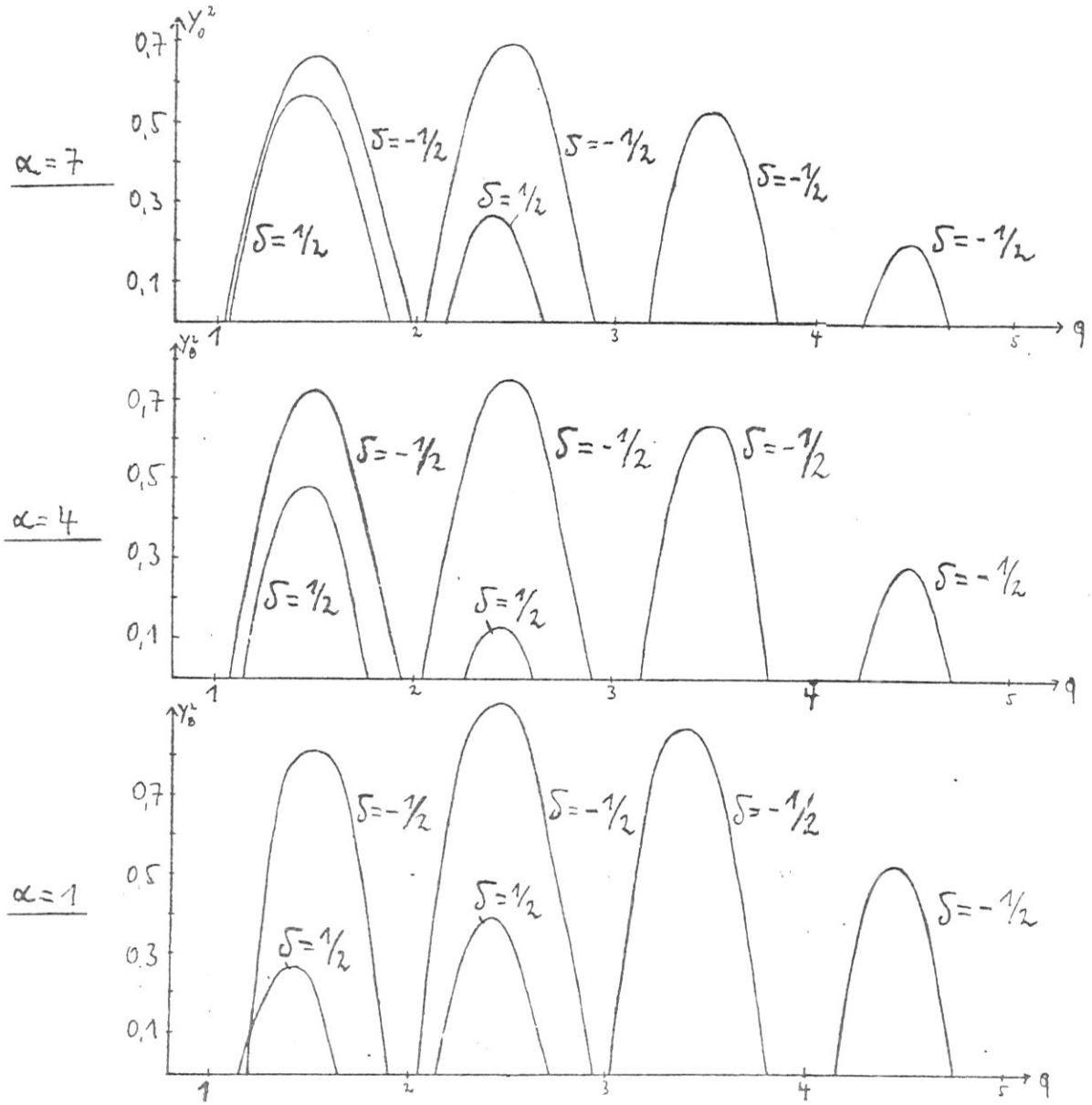

Diagram 14. The Normalized Growth Rate as a Function of the Safety Factor q for Aspect Ratio $\epsilon^{-1} = 8$ without Poloidal Current ($\delta = 0$); – $\Lambda = 2$, --- $\Lambda = 1, 2$.

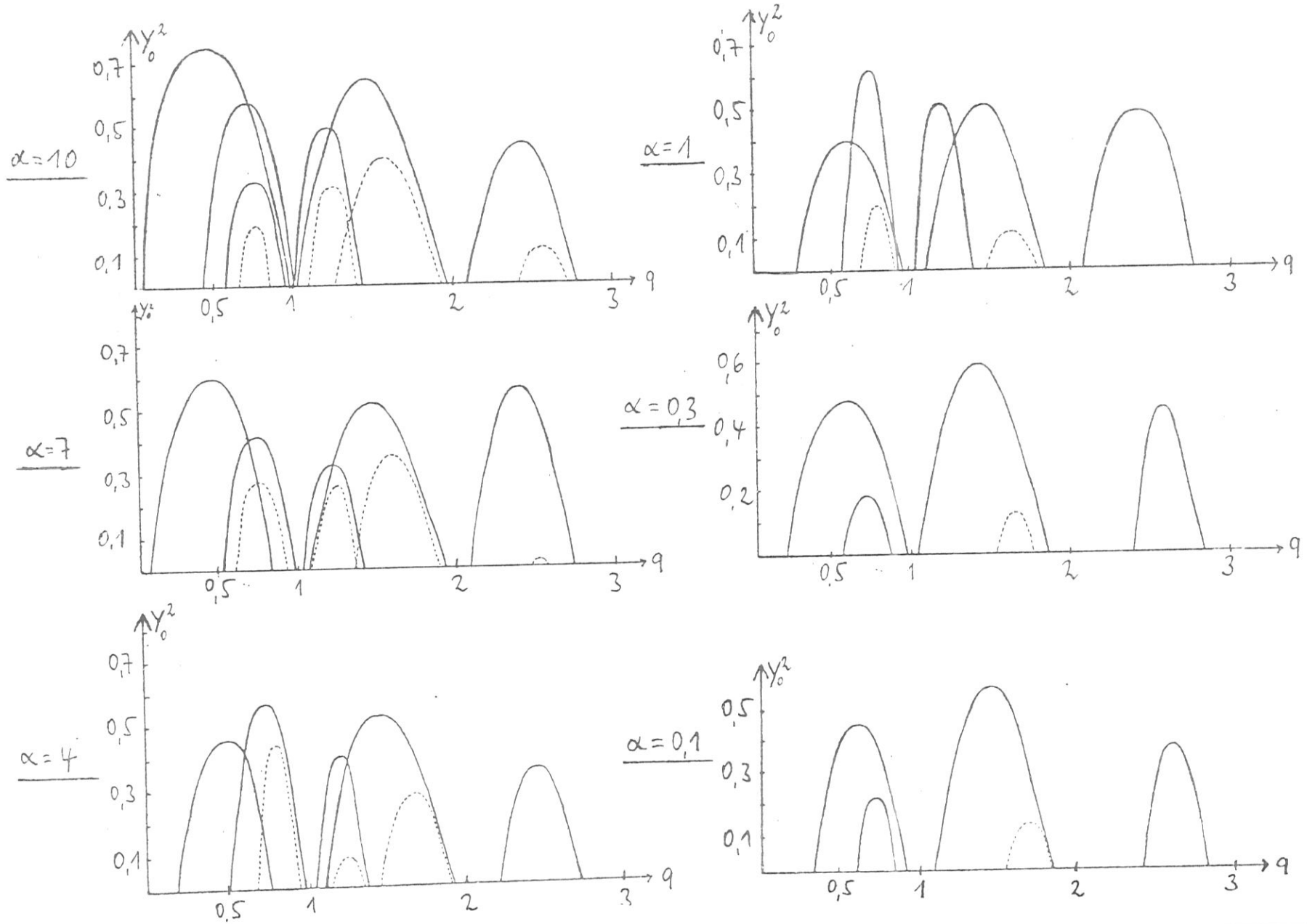

Diagram 15. The Normalized Growth Rate as a Function of the Safety Factor q for Aspect Ratio $\epsilon^{-1} = 8$ with Poloidal Current ($\delta = -1$) ; – $\Lambda = 2$, --- $\Lambda = 1, 2$.

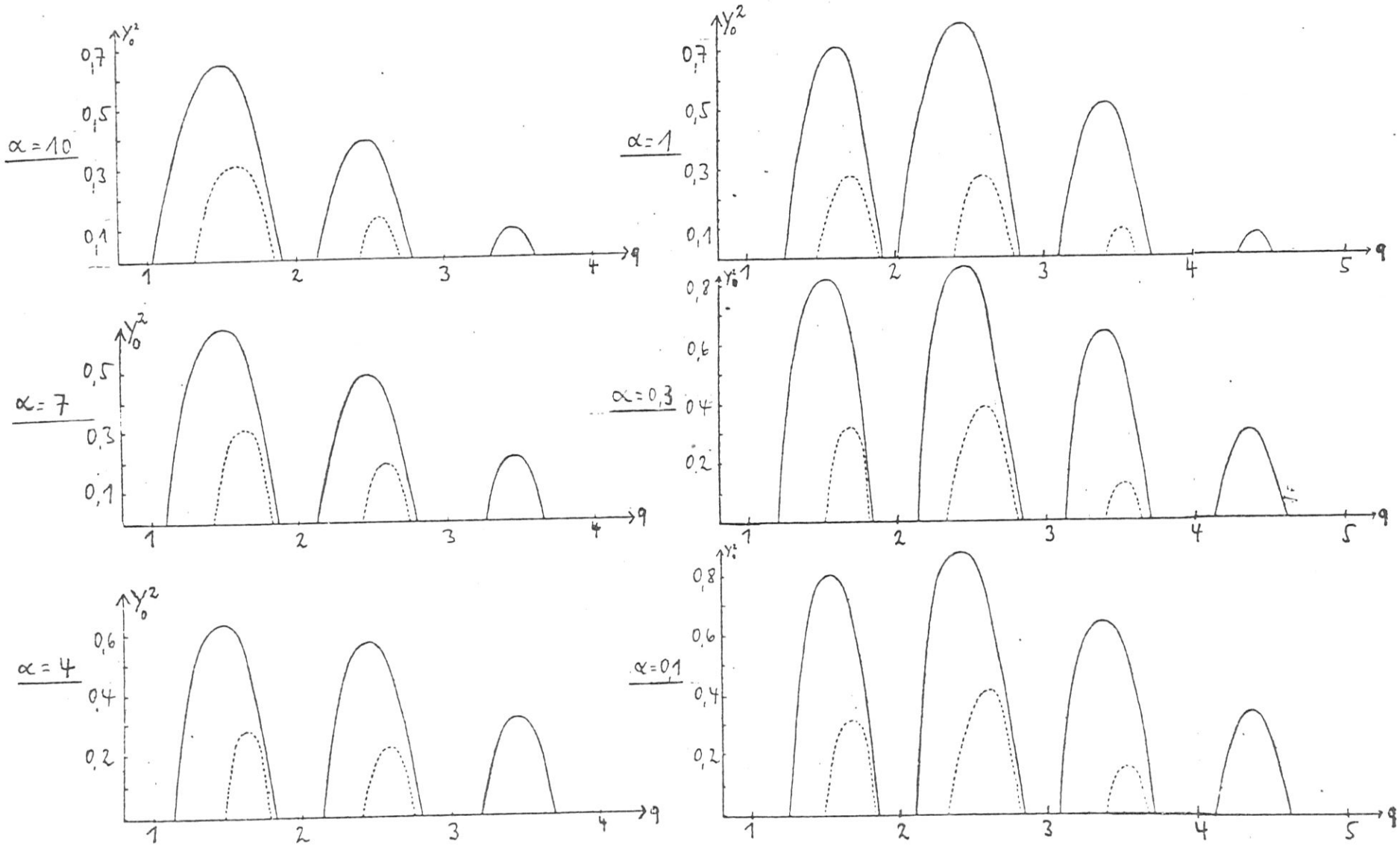

Diagram 16. The Normalized Growth Rate as a Function of the Safety Factor q for Aspect Ratio $\epsilon^{-1} = 6$ without Poloidal Current ($\delta = 0$); $\Lambda = 2$.

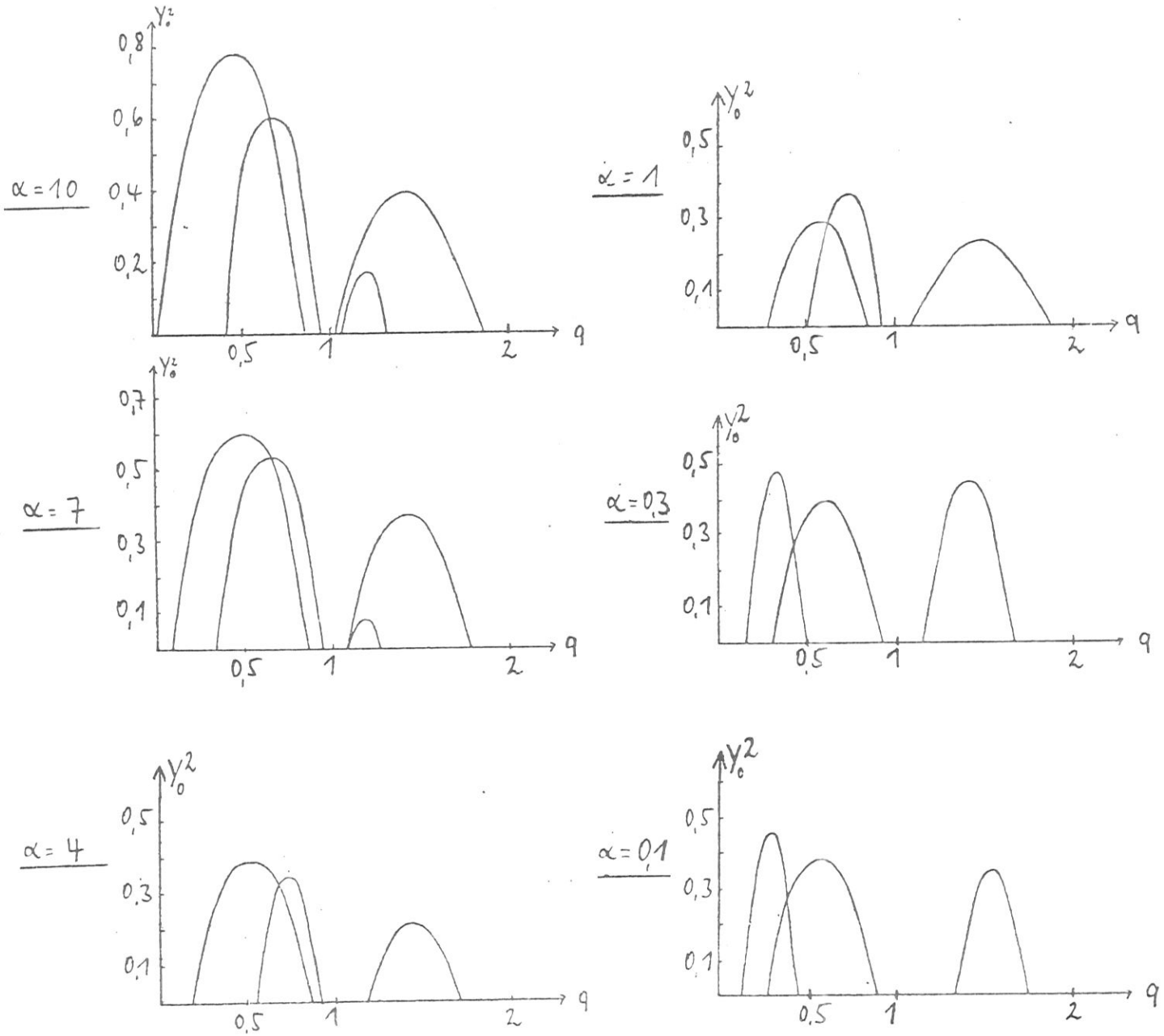

Diagram 17: The Normalized Growth Rate as a Function of the Safety Factor with Poloidal Current ($\delta = -1$); $\Lambda = 2$.

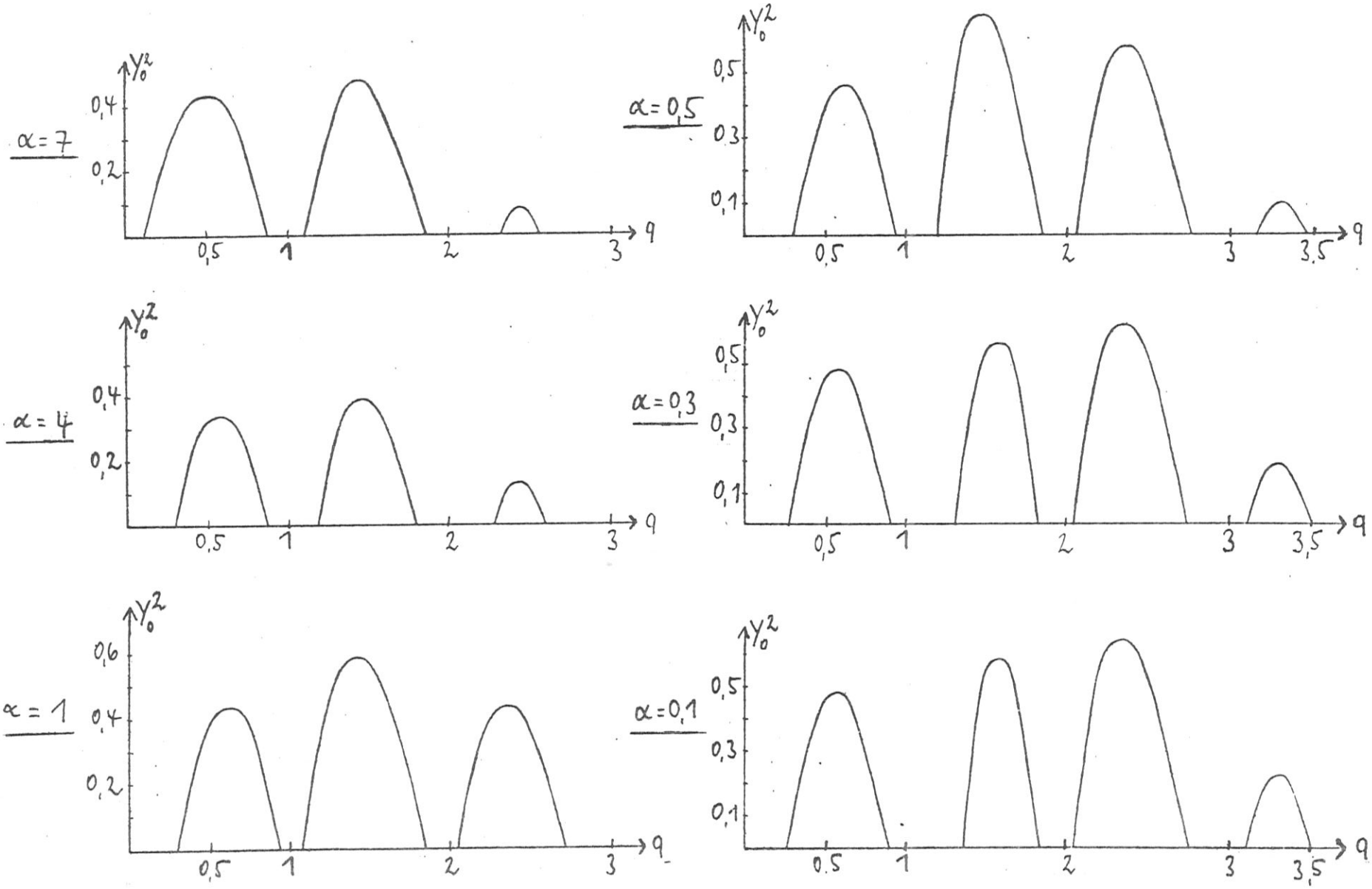

Diagram 18. The Normalized Growth Rate Y_o^2 as a Function of the Safety Factor without Poloidal Current ($\delta = 0$) for Fixed Plasma Boundary.

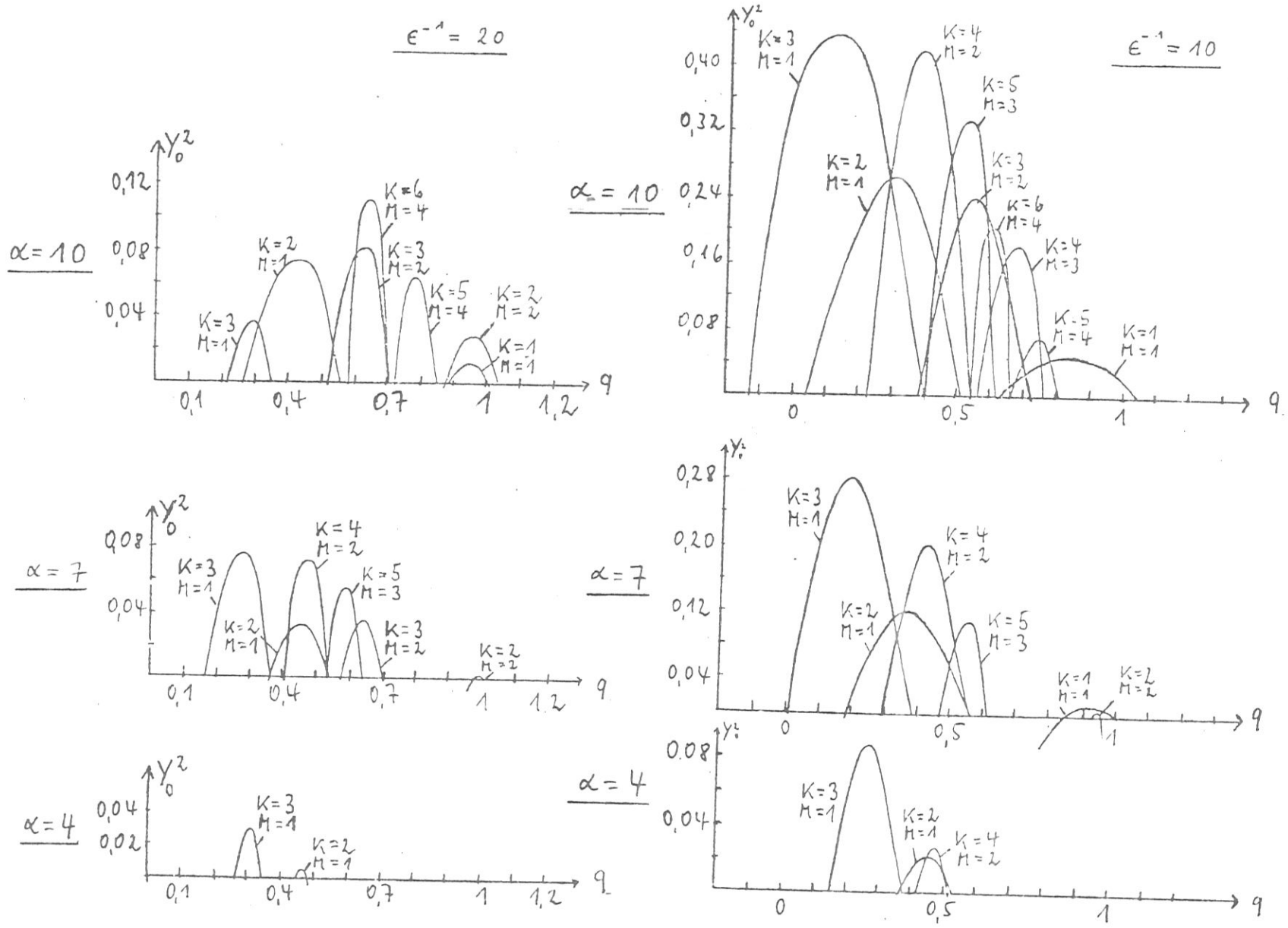

Diagram 19. The Normalized Growth Rate Y_o^2 as a Function of the Safety Factor with Poloidal Current, $\epsilon^{-1} = 20$, for Fixed Plasma Boundary .

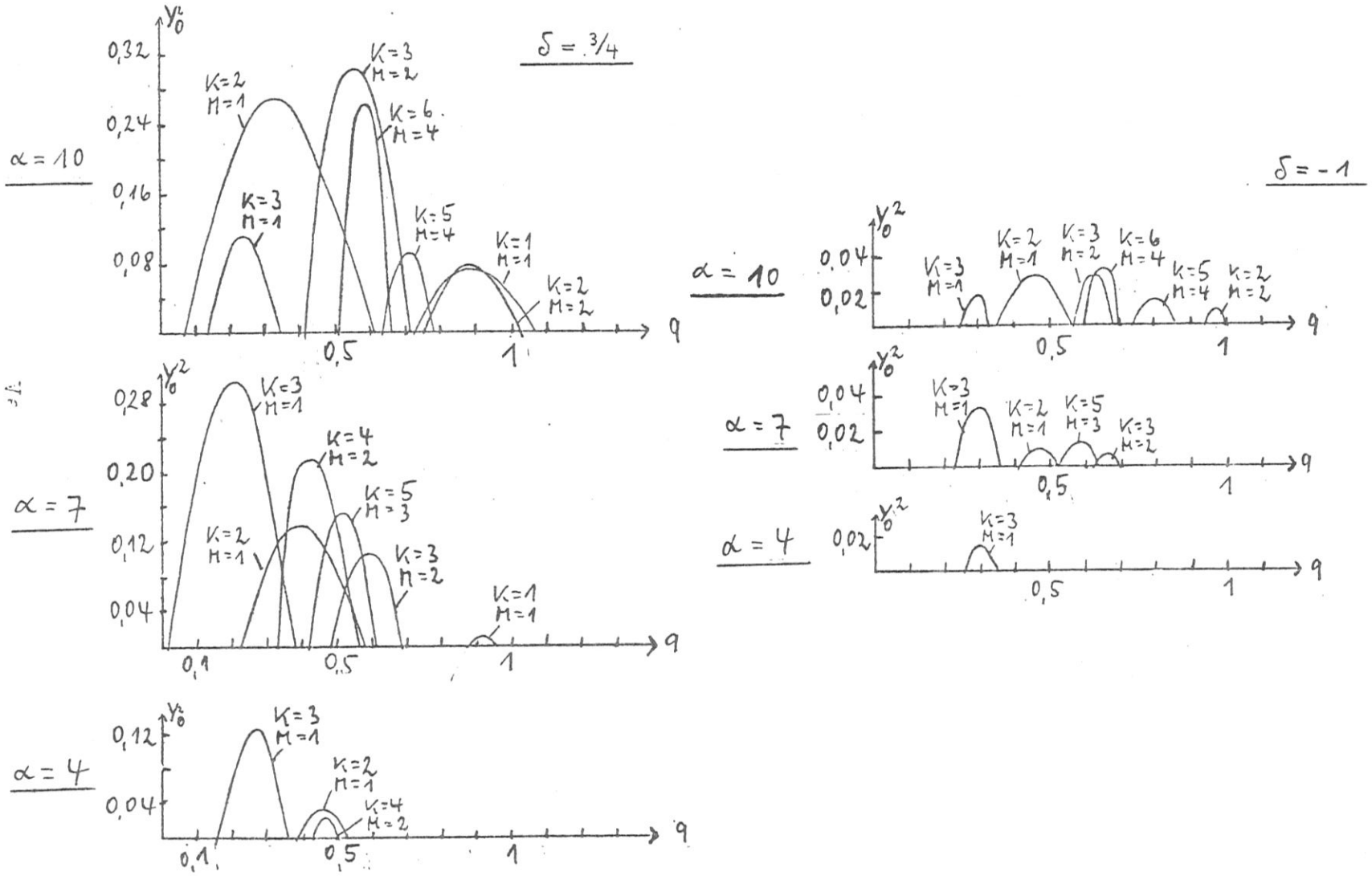

Diagram 20. The Normalized Growth Rate Y_o^2 as a Function of the Safety Factor with Poloidal Current, $\epsilon^{-1} = 10$, for Fixed Plasma Boundary.

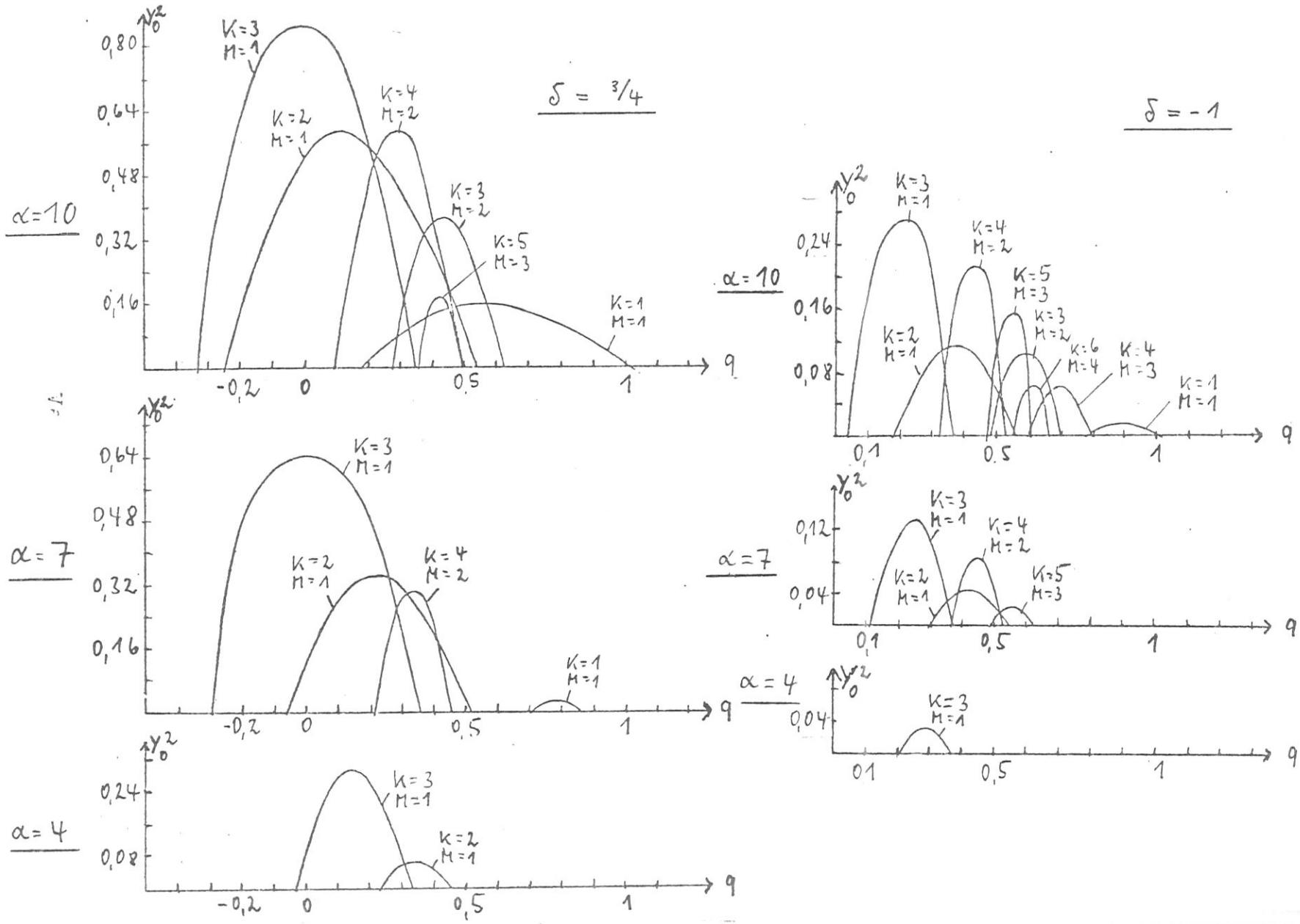

Diagram 21. The Normalized Growth Rate Y_o as a Function of the Safety Factor without Poloidal Current ($\delta = 0$).